Nano-Micro Letters

ISSN 2311-6706
e-ISSN 2150-5551
CN 31-2103/TB

REVIEW

https://doi.org/10.1007/s40820-021-00738-9

Cite as
Nano-Micro Lett.
(2021) 13:216

Received: 16 August 2021
Accepted: 13 September 2021

Recent Advances in Interface Engineering for Electrocatalytic CO_2 Reduction Reaction

Junjun Li[1], Sulaiman Umar Abbas[1], Haiqing Wang[2] ✉, Zhicheng Zhang[1] ✉, Wenping Hu[1]

HIGHLIGHTS

- This review summarizes current developments in interface engineering for electrocatalytic CO_2 reduction reaction (CO_2RR).
- The interface engineering for electrocatalytic CO_2RR involves the metal–metal interface, metal–metal oxide interface, metal–nonmetal interface, metal oxide–metal oxide interface, organic molecules–inorganic materials interface, electrode–electrolyte interface, and molecular catalysts–electrode interface.
- The opportunities and challenges of interface engineering for CO_2RR are proposed.

ABSTRACT Electrocatalytic CO_2 reduction reaction (CO_2RR) can store and transform the intermittent renewable energy in the form of chemical energy for industrial production of chemicals and fuels, which can dramatically reduce CO_2 emission and contribute to carbon-neutral cycle. Efficient electrocatalytic reduction of chemically inert CO_2 is challenging from thermodynamic and kinetic points of view. Therefore, low-cost, highly efficient, and readily available electrocatalysts have been the focus for promoting the conversion of CO_2. Very recently, interface engineering has been considered as a highly effective strategy to modulate the electrocatalytic performance through electronic and/or structural modulation, regulations of electron/proton/mass/intermediates, and the control of local reactant concentration, thereby achieving desirable reaction pathway, inhibiting competing hydrogen generation, breaking binding-energy scaling relations of intermediates, and promoting CO_2 mass transfer. In this review, we aim to provide a comprehensive overview of current developments in interface engineering for CO_2RR from both a theoretical and experimental standpoint, involving interfaces between metal and metal, metal and metal oxide, metal and nonmetal, metal oxide and metal oxide, organic molecules and inorganic materials, electrode and electrolyte, molecular catalysts and electrode, etc. Finally, the opportunities and challenges of interface engineering for CO_2RR are proposed.

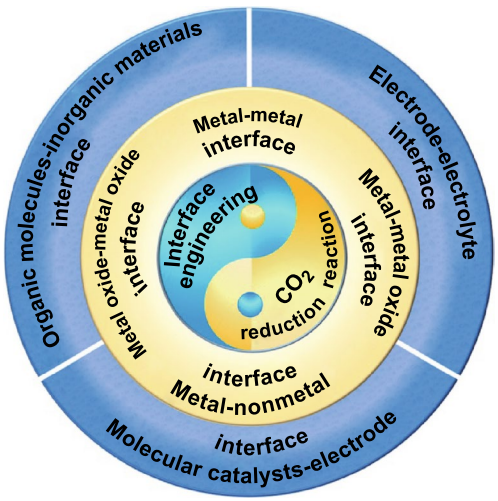

KEYWORDS Interface engineering; CO_2 reduction reaction; Electrocatalysis; Heterostructure

✉ Haiqing Wang, ifc_wanghq@ujn.edu.cn; Zhicheng Zhang, zczhang19@tju.edu.cn
[1] Tianjin Key Laboratory of Molecular Optoelectronic Sciences, Department of Chemistry, School of Science, Tianjin University and Collaborative Innovation Center of Chemical Science and Engineering, Tianjin 300072, People's Republic of China
[2] Institute for Advanced Interdisciplinary Research (iAIR), University of Jinan, Jinan 250022, People's Republic of China

Published online: 25 October 2021

1 Introduction

The combustion of fossil fuels into the atmosphere liberates significant volume of greenhouse gases, resulting in the continuous gathering of CO_2 and an imbalance in the carbon cycle [1–13]. The current overall concentration of CO_2 in the airspace reached up to 416.96 ppm in 2021 [14]. The overconcentration of CO_2 in the atmosphere has crucial negative impacts on the climate and environment, such as climate warming, ocean acidification, and glaciers thaw, which will impact the survival and development of human beings seriously [15–18]. Until now, the conversion of CO_2 to value-added chemicals and fuels is a promising solution to reducing the emission of CO_2 [19–27]. Among various CO_2 conversion techniques (electrocatalysis [28–37], photocatalysis [38–45], thermocatalysis [46], biochemical reduction [47, 48], mineralization [49–51], chemical reforming [52–54], etc.), the electrochemical technique has been considered as an effective strategy for its mild operation conditions, clean reaction process, and wide range of reduction products [55–59]. In addition, this process can be powered by renewable energies such as solar, wind, and tide, thus fulfilling the storage of electricity generated from intermittent renewable green energy [60–71]. Therefore, the electrocatalytic CO_2 reduction (CO_2RR) offers a sustainable and carbon-neutral route to generate high value-added fuels and feedstocks.

In recent decades, researches about CO_2RR have been focused on understanding the electrocatalytic pathways, the properties of electrocatalysts, the configuration of electrochemical cell, and the economic feasibility for large-scale production. Specifically, a typical CO_2RR process mainly includes three steps, i.e., the chemisorption of CO_2 from electrolyte to the surface of electrocatalyst, the breaking of C–O bonds and/or the formation of C–H bonds through electron transfer and/or protonation process, and the desorption of rearranged product species from the surface of catalyst into electrolyte [72]. However, due to the high bonding energy (750 kJ mol^{-1}) of the C=O double bond and the low solubility of CO_2 in water, CO_2 reduction is an energy consuming and kinetically slow process [73]. In the step of transfer of electrons and protons, CO/HCOOH, HCHO, CH_3OH, and CH_4 are formed correspondingly with the consumption of 2, 4, 6, and 8 electrons during the reaction. In contrast to the C_1 products, the C_{2+} products are generally formed via a complex carbon–carbon (C–C) coupling reaction. Although exciting advances have been made in the field of CO_2RR, its development is still suffering from the low yield and unsatisfactory Faradaic efficiency (FE), owing to the chemical inertness of CO_2 molecule, the sluggish reaction kinetics, the competition between hydrogen evolution reaction (HER) and CO_2RR, and the scaling relation of the binding energy for reaction intermediates [74, 75]. Energy-efficient, highly selective, and readily available electrocatalysts are highly desired to solve above-mentioned problems, which fundamentally requires the design, modification, optimization of catalyst materials, and the disclosure of significant mechanism through theoretical calculation and in situ spectroscopic analyses.

In recent years, interface engineering has brought novel and exciting possibilities, such as confinement, electronic, and synergistic effects, to improve catalytic properties through intense interactions between different components [76]. An interface is the boundary between two domains that facilitates interactions and synergistic effects among various active actors, resulting in remarkable ability in modulating intermediate adsorption/desorption, managing electron transmission, and mass movement [76, 77]. With the fast advancement of nanotechnology, it is believed that interface engineering would develop into a successful technique to address the important issues and thus to improve catalytic activity, selectivity, and stability.

The primary purpose of this review is to provide a comprehensive overview of current development in the interface engineering for CO_2RR from both a theoretical and experimental standpoint, involving interfaces between metal and metal, metal and metal oxide, metal and nonmetal, metal oxide and metal oxide, organic molecules and inorganic materials, electrode and electrolyte, molecular catalysts and electrode, etc. (Fig. 1). Finally, the opportunities and challenges of interface engineering for CO_2RR are proposed.

2 Reaction Pathways and Key Scientific Issues of CO_2RR

In recent review articles, the measurement system for CO_2RR including cell configuration, electrochemical measurements and catalytic activity descriptors, products

https://doi.org/10.1007/s40820-021-00738-9

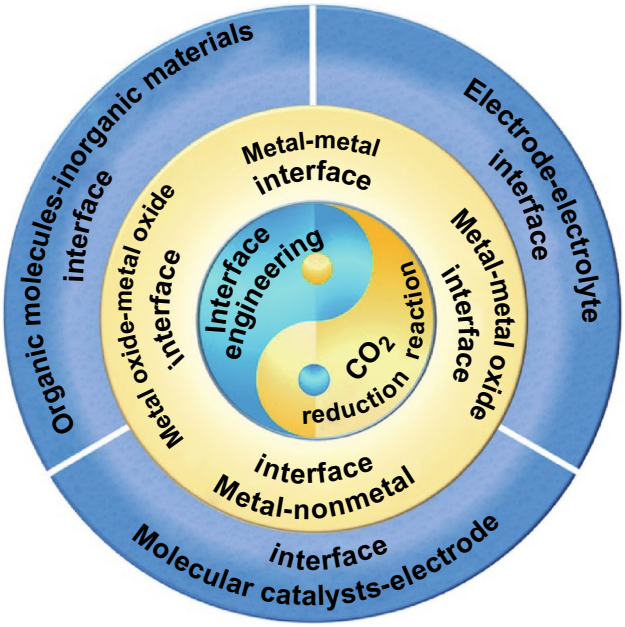

Fig. 1 Schematic overview of interface catalysis in electrochemical CO_2RR covered in this review

detection, and the techniques for monitoring reaction pathways has been comprehensively proposed. Especially, the reaction mechanism and the pathways for C_1, C_2, and C_3 productions of CO_2RR have been comprehensively investigated based on in situ characterization and theoretical calculations, although some detailed parts are still controversial. Here, we focus on revealing the key scientific issues encountered in CO_2RR research by briefly explaining the representative pathways in order to inspire the subsequent studies on CO_2RR (Scheme 1).

2.1 High Energy Input

Owing to a high bonding energy of about 750 kJ mol^{-1} in C=O bond, CO_2 molecules have high thermodynamic stability and chemical inertness, indicating that CO_2RR requires more energy to break the C=O bond. As a result, the starting step of first electron transfer to generate CO_2^- radical usually requires a more negative redox potential of − 1.9 V versus standard hydrogen electrode, which is widely considered as the rate-determining step for CO_2RR. Besides, CO_2RR also contains complex reaction processes with multiple electrons and protons transfer, which implies kinetically sluggish processes. For future industrial-scale applications, it is important to develop highly efficient CO_2RR catalysts to achieve lower energy consumption and faster reaction kinetics.

2.2 Undesirable Competing HER

As mentioned above, CO_2RR usually requires the participation of protons, and the species in the electrolytes such as water, bicarbonate, hydronium ions, and carbonic acid can be used as proton sources. According to the theoretical calculation results, the binding energy of adsorbed hydrogen needs to match the binding energy of C-binding intermediates for hydrocarbon conversion; otherwise, hydrogen will first combine to form hydrogen gas, resulting in much lower selectivity. As a result, the HER is undesirable and competing over CO_2RR, and selective HER inhibition is an urgent issue for CO_2RR.

2.3 Linear Scaling Relation

Based on the available reaction pathways, it is known that the different products generally have the same initial or in-process intermediates. For example, *CO is generally considered to be the common initial intermediate for most of the products including CO, alkanes, and alcohols. And for the pathways of C_{2+} chemicals such as CH_3COOH, C_2H_4, and C_2H_5OH, it usually undergoes complex joint *CO–CO or its protonated form from the very initial *CO. Moreover, *CHO is recognized to be the in-process intermediate for CH_4 and CH_3OH generation, which is then converted to different final products according to the difference of their binding energy with the catalyst surface, respectively. In addition, there is a linear scaling relation in the binding energies of different intermediates on the catalyst surface. In other words, the binding affinities of different intermediates involved in the reaction are similar, resulting in difficulty in controlling their adsorption and desorption modulation. Therefore, it is very challenging to obtain single products with high FE and high selectivity, especially multi-carbon products.

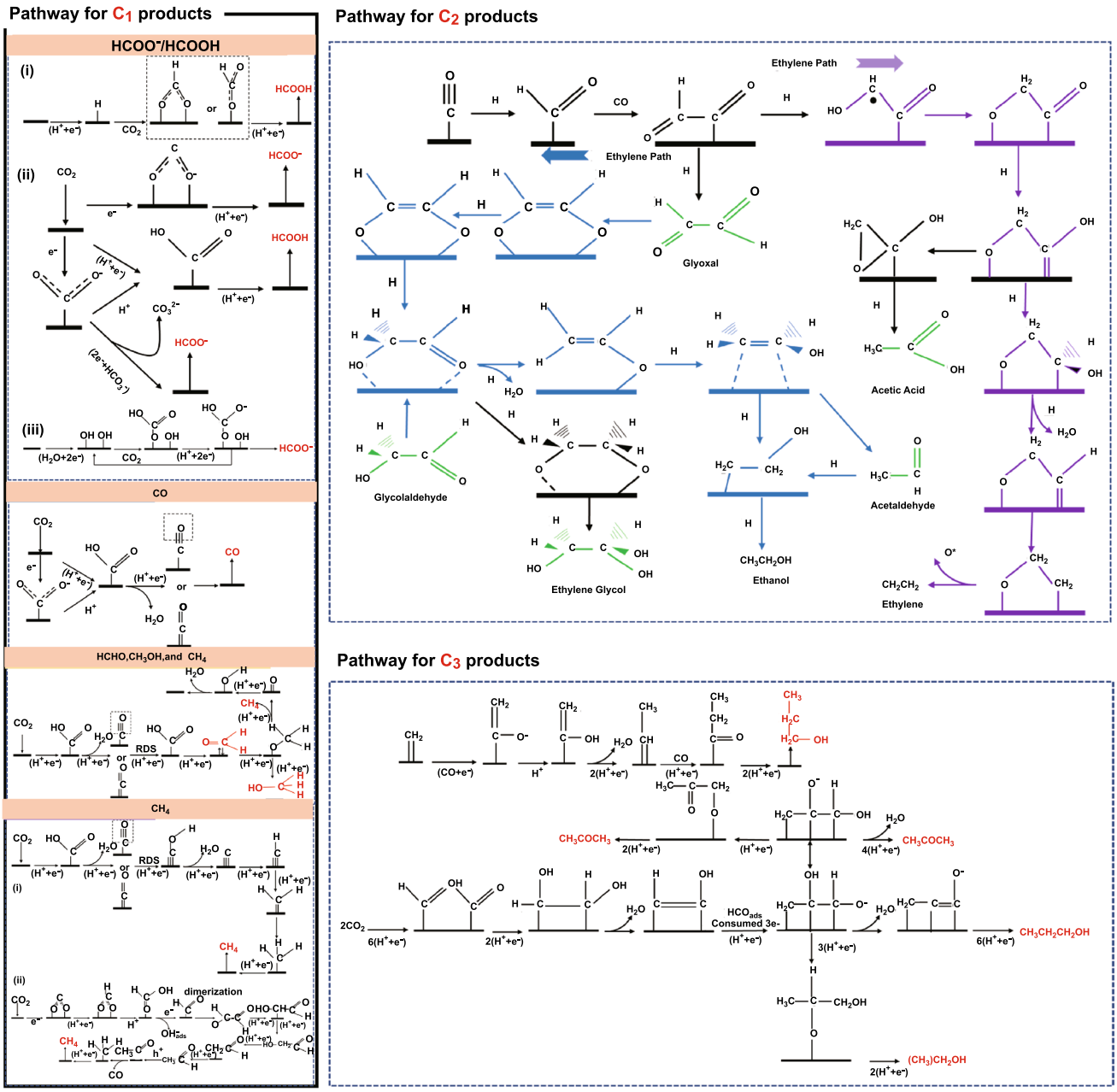

Scheme 1 Overview of the possible reaction pathways of CO_2RR for C_1, C_2, and C_3 products. Reprinted with permission from Ref. [78]

2.4 Low CO_2 Concentration Limitations

For CO_2RR, CO_2 molecules are used as a carbon source. Normally, CO_2 gas is continuously passed into the electrolyte, which dissolves and forms a CO_2-saturated solution. Then, CO_2 molecules migrate to the cathode surface by convection or diffusion to form CO_2RR products via proton and electron transfer. CO_2-saturated $KHCO_3$ solution is a commonly used electrolyte, in which the pH in the bulk is in the range of 6.8 to 7.2 and the concentration is estimated to be about 33 mM. Currently, the low CO_2 solubility and the slow interfacial transport greatly limit the efficiency of CO_2RR. Increasing the local concentration of CO_2 on the electrode surface through some strategies such as reaction cell configuration design (e.g., flow cell), electrolyte screening, electrode and electrolyte interface,

 https://doi.org/10.1007/s40820-021-00738-9

and electrode and gas interface is important to improve the electrocatalytic efficiency of CO_2.

3 Interface Engineering for CO_2RR

Among various reported strategies to address the aforementioned problems for CO_2RR, such as particle size, crystal surface, morphology, and defects, interface engineering has the advantage of being extremely rich and adjustable for regulating reaction processes. From the perspective of a loaded catalyst, the phases that make up the interface can be viewed as the loading phase and the supporting phase. The interface is able to contribute to the dispersion and the stability of both two domains. Moreover, compared to the bulk phase atoms, the atoms located at the interface of the object are in a coordination unsaturated state, which are usually the active sites for the reactions and prone to the physisorption, chemisorption, or direct chemical reactions with other species to generate new species. In addition, the interface shows very significant advantages in regulating bonding energy, electron transfer, transformation and transport of adsorbates and intermediates, which still needs to be studied more carefully. Several principles (the compatibility of materials, electrophilicity of each component, the conductivity after the composition and the variation of electronic distribution on the surface and interface) should be taken into consideration for fulfilling better electrocatalytic performance [79].

3.1 Metal–Metal Interface

Recently, integrating the second metals to construct metal–metal interface has attracted wide attention due to the cooperative effects of bimetal species at the interface [80]. Among all metals, Cu, thanks to its unique electronic properties, has become the most effective monometallic catalyst for CO_2RR to convert CO_2 to various hydrocarbons and oxygenates, such as methane, ethylene, methanol, ethanol, and C_{3+} products [81–89]. Moreover, the features of high activity, low toxicity, and high abundance [90] enable the Cu to commercialize CO_2RR. However, the present issues, such as low selectivity toward a specific product and low FE due to competition with HER and sluggish kinetics, still need to be addressed [76, 81, 84, 85, 90, 91]. In recent years, various interface-related strategies have been devised to enhance its catalytic performance, such as intermetallic compounds [92], heteroatomic doping [68, 93], single Cu atom catalysts [94], core–shell structures [86], and heterostructure [95–97]. Among them, alloying is a general and widespread method to improve catalytic performance [98–100]. However, the intrinsic electronic properties of the component metals will be significantly modified after alloying. By contrast, constructing metal–metal interface can, to some extent, preserve the intrinsic feature of the metals [101], which is in favor of realizing high electrocatalytic performance [101–103].

For example, Wang et al. constructed exposed Ag/Cu interface by distributing Ag nanoparticles on the surface of Cu nanoparticles (Fig. 2a) [82]. The electrocatalytic performance of four catalysts (Ag/Cu, AgCu alloy, pure Cu, and Ag NPs) was compared for CO_2RR (Fig. 2b). It is obvious that Ag/Cu catalyst exhibited maximum FE of 42% toward C_2H_4 at − 1.1 V versus reversible hydrogen electrode (vs. RHE), obviously superior to the other three catalysts. Further, they proposed a detailed process to explain how the interface facilitates the production of C_2H_4. As shown in Fig. 2c, CO, the key intermediate for hydrocarbons, is obtained on Ag atoms after the following two-step electron and proton transfer process:

$$CO_2 + {}^{*} + \left(H^{+} + e^{-}\right) \rightarrow {}^{*}COOH$$

$${}^{*}COOH + \left(H^{+} + e^{-}\right) \rightarrow {}^{*}CO + H_2O$$

Then, CO species that transfer to Cu atoms can further couple into C_2H_4 via continuous proton–electron transfer. Owing to higher CO binding energy of Cu than that of Ag, CO intermediates accumulate in large quantities at the interface which is in favor of the formation of C–C bond by coupling, i.e., a rate-determining step for C_{2+} production. As for AgCu alloy, the existence of a transition AgCu layer is suggested to depress the process of CO dimerization, consequently resulting in low selectivity of C_2H_4.

Almost at the same time, Huang et al. further explored and illustrated interface effect between Cu and Ag for CO_2RR [83]. They synthesized Ag–Cu nanodimers (NDs) (Fig. 2d) by using Ag nanoparticles as nucleation seeds, which apparently outperformed pure Ag and Cu NPs in terms of FE of C_2H_4. Particularly, Ag_1–$Cu_{1.1}$ NDs (mass ratios) exhibited FE of approximate 40% toward C_2H_4 at − 1.1 V versus RHE, a 3.4-fold enhancement compared with pure Cu NPs (Fig. 2e). Combining with previous reports [104–106], they speculated that the Ag domain serves as supplier of CO to adjacent Cu domain, and meanwhile, Cu supplies electron to

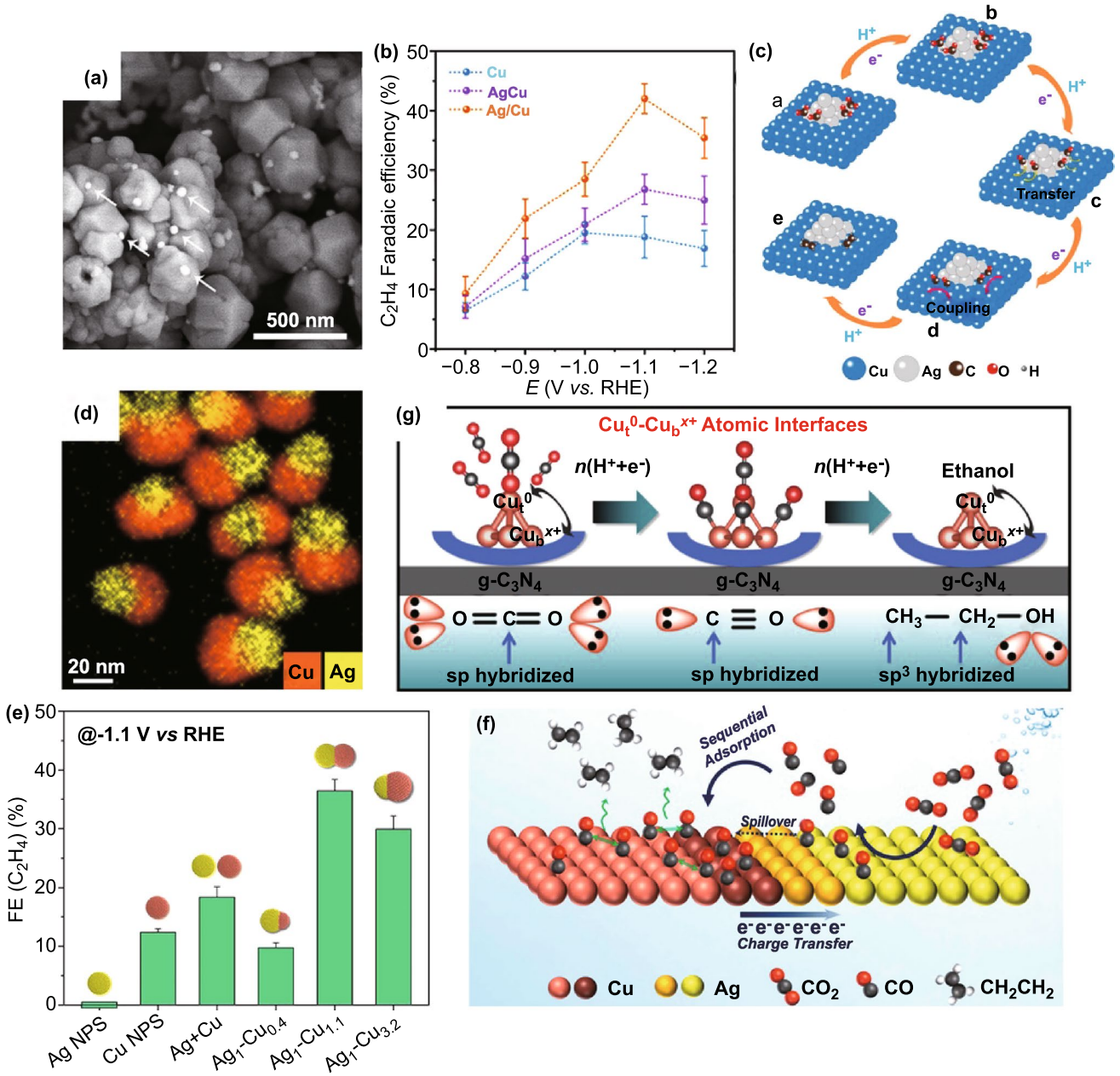

Fig. 2 **a** Scanning electron microscope (SEM) image of Ag/Cu_2O. **b** FE of C_2H_4 for Ag/Cu_2O catalyst. **c** Mechanism for converting CO_2 to C_2H_4 on Ag/Cu interface. Reprinted with permission from Ref. [82]. **d** EDX elemental maps of Ag_1–$Cu_{1.1}$ NDs. **e** FEs of C_2H_4 obtained on different Ag/Cu nanocrystals. **f** The tandem catalysis mechanism of C_2H_4 promotion in the Ag–Cu NDs. Reprinted with permission from Ref. [83]. **g** Schematic of mechanism for conversion to CH_3CH_2OH on Td-Cu_4@g-C_3N_4. Reprinted with permission from Ref. [108]

Ag. Subsequent control experiment that employed Ag + Cu mixture (a physical mixture of Ag NPs and Cu NPs) as catalyst verified their hypothesis with density functional theory (DFT) analysis, X-ray diffraction pattern, and X-ray photoelectron spectroscopy (XPS) spectra. In particular, they pointed out that the tandem effect and electronic effect result from the coupling of Ag and Cu nanodomains at their interface (Fig. 2f). Later, Hou et al. further confirmed above conjecture with Ag nanoparticle embedded Cu nanoporous hybrid arrays as model via theoretical calculations [81]. The modified Ag NPs could regulate the electron structure of porous copper at the Cu/Ag interface, which is in favor of the

 https://doi.org/10.1007/s40820-021-00738-9

first process of electron transfer to form *CO, and facilitate the adsorption and conversion of *CO to ethylene.

Recently, the researches on atomic scale have received more attention, which partly is ascribed to an essential role of atoms at (or around) the interface, and more importantly, it is conducive to deep insight about electrocatalysis mechanism [76]. Jiao et al. for the first time, proposed atom-pair catalyst for CO_2RR with FE of CO up to 92% and almost completely suppressed HER [94] and offered a novel and efficient method to construct functional atomic interface at atomic level. The obtained atom-pair catalyst possessed stable Cu_1^0–Cu_1^{x+} pair structures, in which Cu_1^0 adsorbs CO_2 and neighboring Cu_1^{x+} adsorbs H_2O. Based on researches on combining Cu^0 and Cu^{x+} as catalysts for CO_2RR reported recently [87, 107], Bai et al. [108] systematically studied the reaction path and proposed a possible mechanism to convert CO_2 to CH_3CH_2OH at the interface between Cu^0 and Cu^{x+} with the as-prepared g-C_3N_4 supported tetrahedral (Td) Cu_4 cluster (Td-Cu_4@g-C_3N_4) as catalyst. As shown in Fig. 2g, owing to higher binding energy, CO_2 molecules tend to be captured by top site of Cu (Cu_t^0) at Cu–Cu atomic interface and then reduced to *CO. The clustered *CO induced by the oxidized Cu_b^{x+} (bottom site of Cu) can be further reduced into *CHO. Subsequently, due to lower reaction free energy, the formation of *OHC–CHO* through C–C coupling takes precedence rather than forming two separated *CHO. Finally, ethanol is obtained after multi-proton–electron transfer process. By applying the excellent activity of Cu^+ to bind *CO, Daiyan et al. constructed Cu^+/Cu^{2+} interface on the Cu sandwich electrode [109]. The results indicate that the Cu^+/Cu^{2+} interface is closely related to the conversion of CO_2 to hydrocarbon, for it can protect Cu_2O species against being reduced during CO_2RR. More importantly, the Cu/Cu_2O interface has also been verified to play an important role in photoelectrocatalysis [90]. A photoelectrochemical cell was constructed with TiO_2 as photoanode, which could improve the stability of Cu_2O at the interface via highly energetic electrons and large potential.

In addition, the interface between Cu and other transition metals (such as Sn [85, 110] and Mo [84]) has also been investigated. Owing to the advantages of low cost, low toxicity, and high selectivity to formate [111–114], Sn has been preferably employed to modify copper-based catalysts [115–119]. Recently, the role of Cu/Sn interface has been investigated in detail [85, 109]. For example, Li et al. pointed out that catalytic performance might be affected by the density of Cu/Sn interface. Later, the research conducted by Li et al. suggested that regulating effect of residual Cu^+ species at the Cu/Sn interface can give rise to an optimal concentration of Sn^{2+} and Sn^{4+} [110], which is prone to formate production [120]. Zang et al. constructed Mo_8/Cu heterostructures, and the as-obtained catalysts demonstrated FE of 48.68% toward acetate and current density of about 110 mA cm^{-2} at − 1.13 V versus RHE. The intrinsic synergetic effect between Mo_8 and Cu at Cu–O–Mo interface was substantiated by the experimental and theoretical results [84].

Apart from Cu, Au has also been widely studied as excellent catalyst, which is liable to generating CO. On account of the high cost of Au, the cheap and plentiful metals are employed as the second metal to reduce the usage amount of Au by constructing Au–metal interface while maintaining or improving catalytic activity. For example, Back et al. investigated Au/Cu interface for CO_2RR, demonstrating the importance of metal–metal interface [101]. Later, Kim et al. elucidated the significance of electronic effect on the Au/Ti interface for enhancing CO_2RR performance [121]. Very recently, Shen et al. built up Fe/Au interface by dispersing isolated Fe atoms on Au NP (Fig. 3a) and tested its electrochemical performance for CO_2RR. The dynamic changes of catalyst were monitored by operando synchrotron radiation spectroscopies [122]. The atomical dispersion of Fe species on Au NPs was verified by microscopy analysis and X-ray absorption fine structure (XAFS) measurements. As shown in Fig. 3b, c, FE of CO for Fe_1/Au reached up to 96.3% at 0.65 V versus RHE with mass activity of 399 mA mg^{-1}, and the TOF of 11,521 h^{-1} at − 0.9 V versus RHE, significantly exceeding that of pure Au. Operando/in situ characterization technique indicated that the enhanced interaction between Fe and Au atoms at the interface promotes charge transfer from Au to Fe and stabilizes the key intermediates *COOH bonding with the O_2-phile Fe atom.

Generally speaking, Au tends to be active to produce CO [123–125]. But its selectivity can be adjusted by introducing different second metals or manipulating their crystal phase [99, 104, 126–128]. For example, Chen et al. prepared the high-purity 4H Au@Cu and the heterophase 4H/fcc Au@Cu via the facile epitaxial growth method under ambient conditions (Fig. 3d) [127]. Different from fcc Cu catalyst, the unconventional crystal phase of Cu exhibited higher activity and selectivity to C_2H_4. The maximum FE is up to 44.9% at − 1.11 V versus RHE and 46.7%

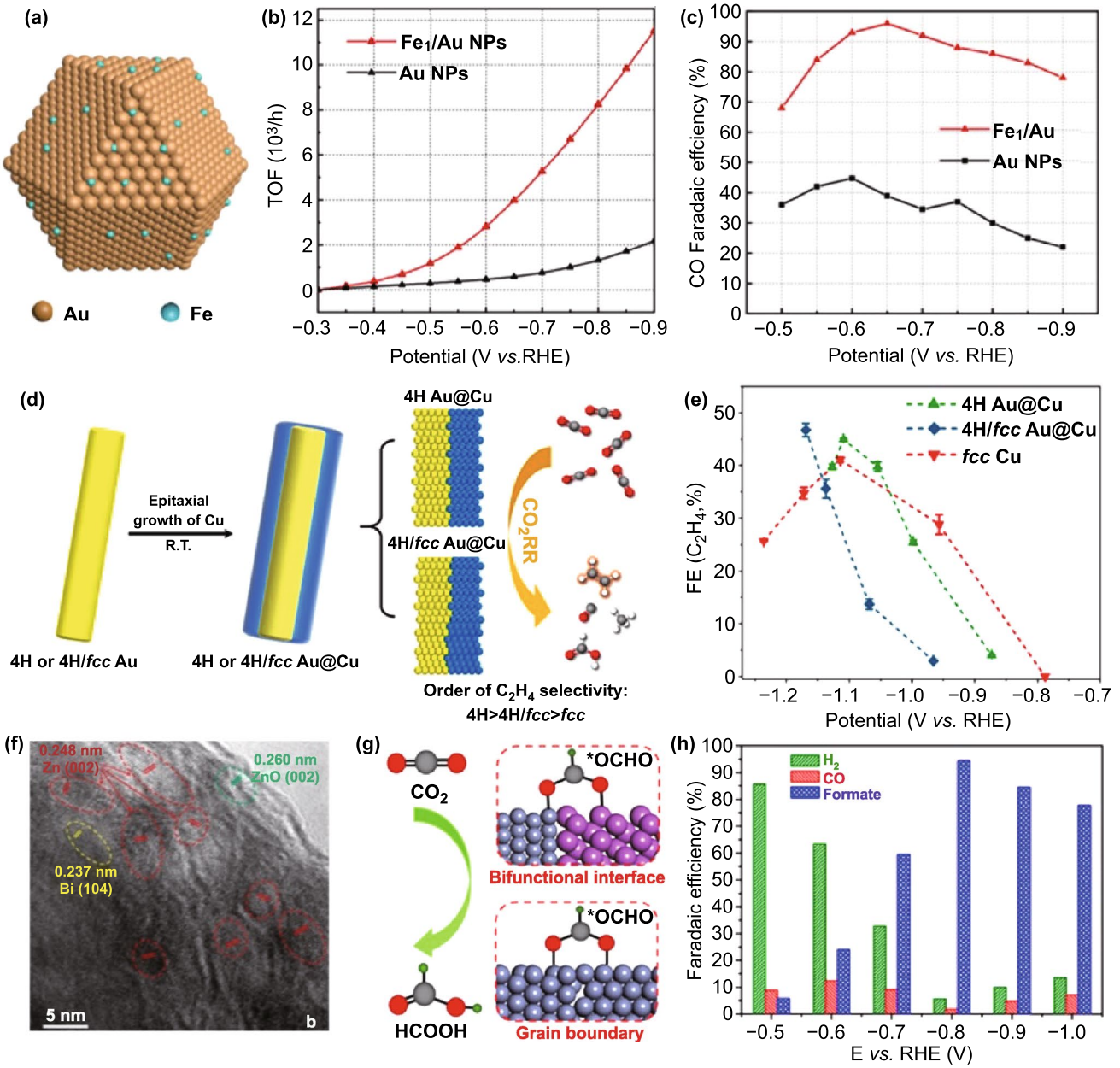

Fig. 3 **a** Schematic diagram of atomically dispersing Fe species on Au NPs. **b**, **c** TOF and FEs of CO for Fe_1/Au and Au NPs. Reprinted with permission from Ref. [122]. **d** Schematic illustration of epitaxial growth of Cu on 4H or 4H/fcc Au nanostructures and their CO_2RR performance. **e** FEs of C_2H_4 on three catalysts. Reprinted with permission from Ref. [127]. **f** High-revolution transmission electron microscope (HRTEM) image of Zn–Bi catalyst. **g** Schematic illustration of catalytic mechanism of Zn–Bi catalyst. **h** FEs of H_2, CO, and formate for Zn–Bi catalyst. Reprinted with permission from Ref. [130]

at − 1.17 V versus RHE, respectively (Fig. 3e). Theoretical calculations demonstrate that there is lower energy barrier to form *CHO thus leading to the easier formation of C_2H_4 at the 4H phase and 4H/fcc interface of Cu than the fcc Cu. Aimed at illustrating bimetallic interfacial effects, Zhang et al. built the interfacial models of the Cu/Au bimetallic system [129]. DFT calculations suggested the enhancement of CO_2RR performance is mainly attributed to the bimetallic interface stress and the lower formation energy of H* at the Cu/Au interface than pure Cu. In addition, the Zn/Bi interface has also been studied [130]. The Bi-modified Zn catalyst with metal–metal bifunctional interface

https://doi.org/10.1007/s40820-021-00738-9

(Fig. 3f) and grain boundaries can provide high density of active sites (Fig. 3g), thus achieving high performance with maximum FE of $HCOO^-$ up to 94% at − 0.8 V versus RHE (Fig. 3h).

3.2 Metal–Metal Oxide Interface

Among various catalysts for CO_2RR, the application of most metal oxides has been largely limited due to poor conductivity [131]. An effective strategy of combing metal oxides with highly conductive metal has attracted increasing interest due to not only the improved electrical conductivity, but also the excellent electrochemical performance [132–136]. In fact, this combination is also conducive to improving the performance of metal itself for CO_2RR [132–134, 137–139]. In brief, the interface between metal and metal oxide synergistically enhances the CO_2RR performance [133].

Take the most commonly used Cu-based catalyst [90, 119, 140, 141] as an example, the unidirectional facilitation has been widely studied. For example, Chang et al. built up structurally controlled Cu/Cu_2O interface (Fig. 4a) via distributing Cu NPs on Cu_2O film [90].

Importantly, the as-obtained interface offers critical active sites for producing CH_3OH. Compared with pure Cu NPs and Cu_2O film, the amount of CH_3OH rises up significantly at the presence of Cu/Cu_2O interface. Especially, the maximum FE can reach up to 53.6% at the longest interface (denoting as E2, Fig. 4b, c), which is one of the highest FEs reported using non-noble catalysts [142, 143]. The FE and the amount of CH_3OH increase with the increasing particle size (Fig. 4d) and interfacial length, respectively. Furthermore, the intrinsic reaction mechanism was investigated with theoretical calculation in terms of thermodynamics and kinetics. Generally, the prerequisite for reducing CO_2

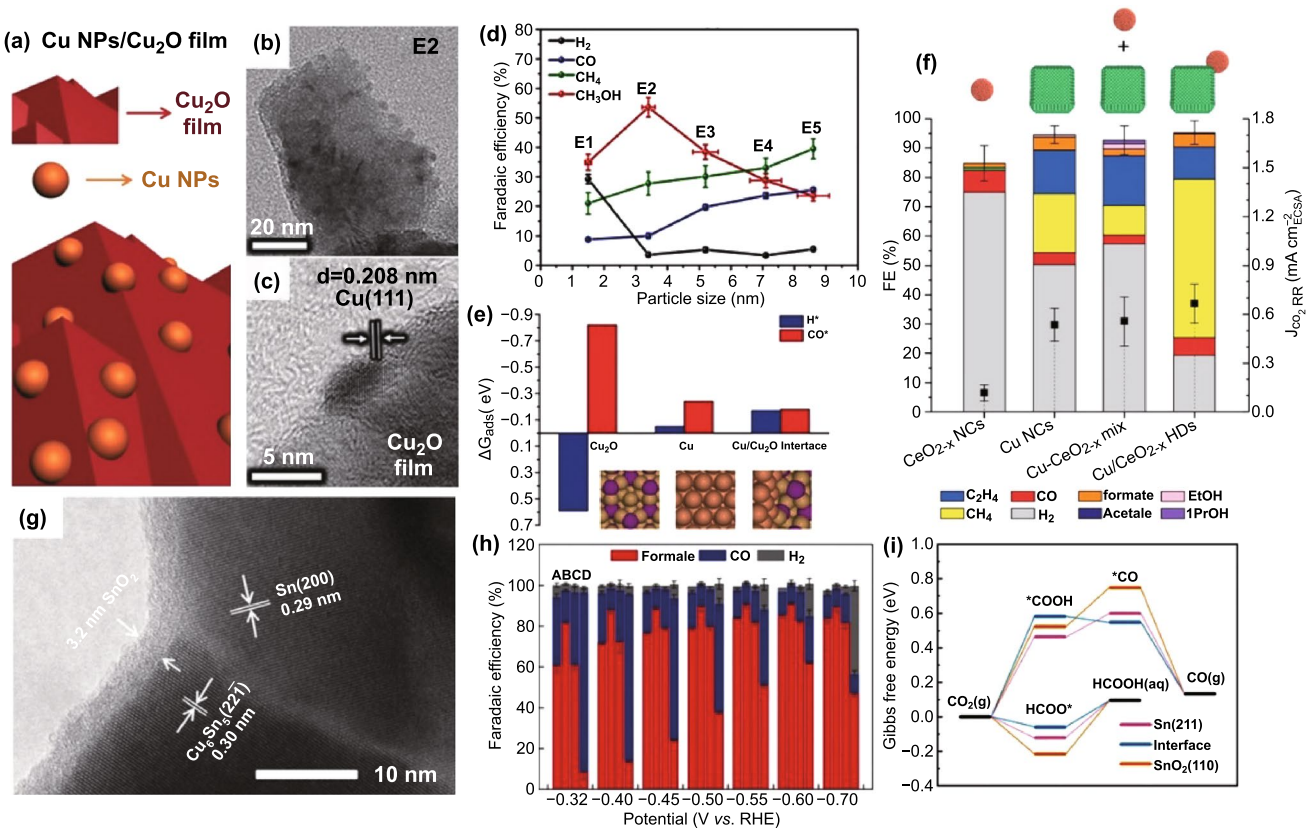

Fig. 4 **a** Schematic representation, **b** TEM and **c** HRTEM images of Cu NPs/Cu_2O film. **d** The dependence of FEs on the Cu NP size. **e** The Gibbs free energies of H* and CO* on different sites. Reprinted with permission from Ref. [90]. **f** FEs and partial current densities for different catalysts. Reprinted with permission from Ref. [141]. **g** HRTEM image of $Sn_{2.7}Cu$ catalyst. **h** FEs of formate, CO, and H_2 for four catalysts. **i** Calculated Gibbs free energy diagrams for CO_2RR on different catalysts. Reprinted with permission from Ref. [137]

to methanol at a high ratio requires stronger H* but weaker CO* binding. As shown in Fig. 4e, the introduced Cu NPs helps to strengthen H* and weaken CO* adsorption at the interface and thus facilitates the formation of CH_3OH. Varandili et al., for the first time, reported the Cu/CeO_x interface for effective CO_2RR by surmounting significant lattice mismatch and poor charge conductivity [141]. In particular, the former can be ascribed to the presence of ligands and solid/liquid interface, which can modulate the interfacial energies and thus make it possible to overcome great mismatch and form heterostructures [144]. Compared with simple physical mixture of Cu and CeO_{2-x} NCs, the as-synthesized Cu/CeO_x catalyst with Cu/Ce^{x+} interface exhibited 5 times higher FE of 54% toward methane at − 1.2 V versus RHE (Fig. 4f). The theoretical model that a ceria nanoparticle is immobilized on Cu-slab based on Graciani et al. was built to explore the interface effect of Cu/CeO_{2-x} [93]. At the microlevel, the enhancement results from bidentate adsorption and stability of CHO* and H_2CO* on Cu and oxygen vacancies in CeO_{2-x}, which is conducive to thermodynamically favored pathway toward C_1 by breaking the CHO*/CO* scaling relationship [145–150]. Afterward, Cu/CeO_2 catalyst with smaller Cu but more ceria NPs was reported to convert efficiently CO_2 to ethylene and ethanol [151]. When Cu and CeO_x NPs were employed to be embedded on carbon nanofibers, the as-obtained Cu/CeO_x@CNFs catalyst exhibited superior activity and selectivity compared to catalysts without Cu/CeO_x interface [140]. The improvement in catalytic performance can be contributed to the synergistic geometric and electronic effects at the Cu/CeO_x interface.

Besides, the enhancement of electrocatalytic performance can also be attributed to the interface forming during the test. For instance, Ye et al. reported the in situ reconstructed Sn/SnO_x interface (Fig. 4g) improved the selectivity toward HCOOH and other C_1 products [137]. Similarly, the Sn/SnO_x interface was constructed through the surface reconstruction before CO_2RR test [120]. As shown in Fig. 4h, among the four catalysts, $Sn_{2.7}Cu$ catalyst with Sn-Cu alloy/Sn core and SnO_2 shell exhibited the highest current density for HCOOH at all measured potentials, and the total current density was up to 406.7 ± 14.4 mA cm^{-2} at − 0.70 V versus RHE. The systematical characterizations of in situ Sn K-edge extended X-ray absorption fine spectra, ex situ XPS spectra and ex situ HRTEM images suggested that the surface SnO_x lessens significantly, which resulted from partial reduction of the SnO_x shell on the surface of $Sn_{2.7}Cu$ catalyst during the electrochemical test. Meanwhile, under the driving of lower surface free energies, the redundant Sn atoms in core spontaneously can transfer to SnO_x shell, and thus, the Sn/SnO_x interface was constructed. Particularly, this phenomenon only exists in $Sn_{2.7}Cu$ catalyst owning to the hierarchically heterogeneous Sn-Cu alloy/Sn core structure. Subsequent DFT calculation revealed that the in situ reconstructed Sn/SnO_x interface can reduce the Gibbs free energy (G) via weakening the binding of HCOO* and then facilitate HCOOH production (Fig. 4i). In addition, the high FE of C_1 production can be partly contributed to superior inhibition of competitive HER, originating from the weakened binding of *H intermediates.

Gao et al. built up Au–CeO_x interface on carbon substrate via loading Au NPs on CeO_x NPs (Au–CeO_x/C) (Fig. 5a) [134]. It demonstrated superior electrocatalytic performance to the pure Au and CeO_x and the mechanism is presented in Fig. 5b. As shown in Fig. 5c, the Au–CeO_x interface showed higher FE of CO generation at all test potentials compared with the pure ones, and the highest FE is up to 89.1% at − 0.89 V versus RHE. Moreover, the geometric current density of CO on Au–CeO_x/C catalyst is 1.6 times higher than those on the two single-component catalysts. In fact, it has been reported that better performance can be achieved when improving utilization of Au NPs electrostatic adsorption process [152]. Contrast experiments showed that hydroxyl groups from the decomposition of water [153] can not only stabilize Ce^{3+} on the surface to facilitate redistribution of oxygen vacancies from bulk to surface [154], but also improve the stability and absorption of $CO_2^{\delta-}$ species at the interface. At the same time, the Bader analysis suggested the presence of interface and hydroxylation can both lead to the reduction of Ce^{4+}. The interaction between Au and Ce^{x+} at the interface makes for the increased concentration of Ce^{3+}. Theoretical analysis showed that the Ce^{3+} species could stabilize *COOH whose formation is limiting step, via direct interaction with terminal oxygen to improve conversion of CO_2 to CO. In addition, the catalysts prepared by substituting Au with Ag were also studied, which similarly demonstrated the improvement in catalysis performance. The research, provided significant instruction for the design of metal-CeO_2 interface as efficient electrocatalysts.

Recently, metal–oxide interface with highly synergistic metal–oxide interactions, for the first time, has been successfully obtained [155]. The as-prepared catalyst consisted of Ag core and SnO_x decorated on the surface of Ag (Fig. 5d).

https://doi.org/10.1007/s40820-021-00738-9

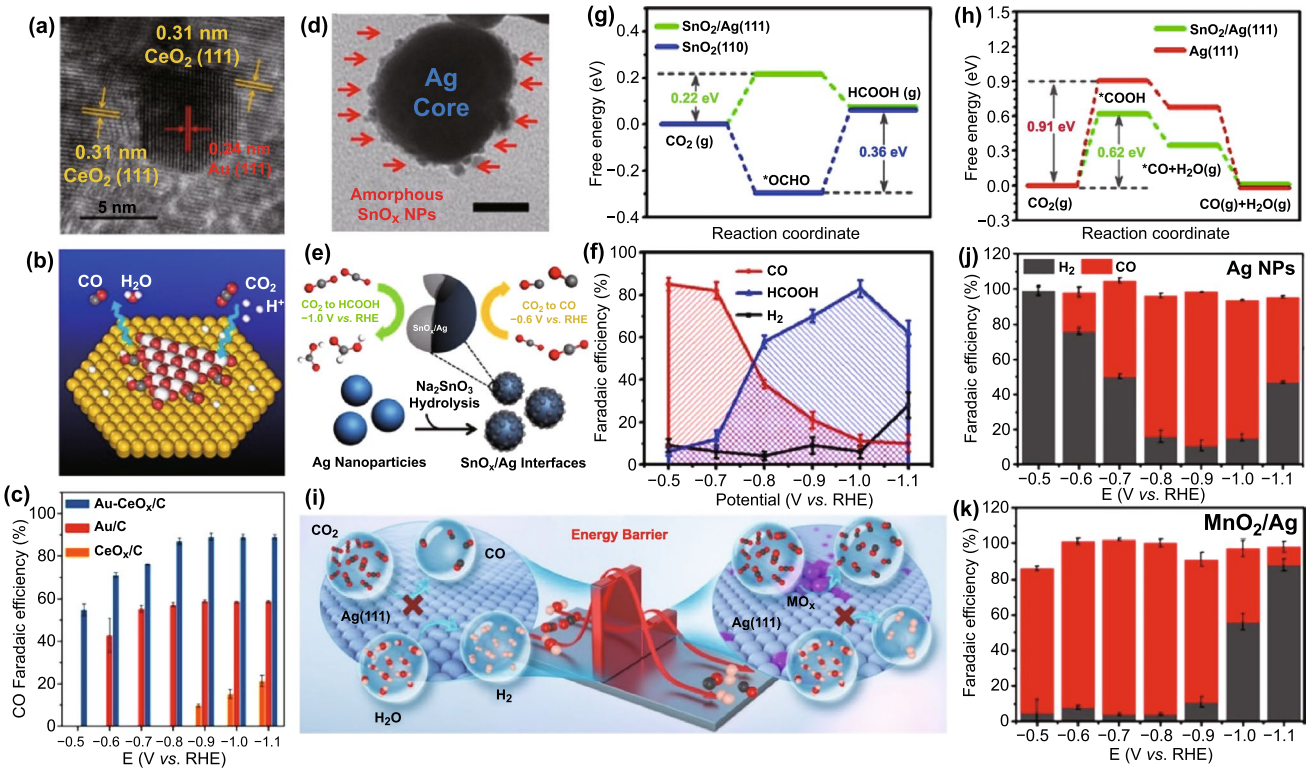

Fig. 5 **a** HRTEM image of Au/CeO_x catalyst. **b** Schematic representation of mechanism of Au–CeO_x/C catalyst. **c** FEs of CO for different catalysts. Reprinted with permission from Ref. [134]. **d** TEM images of SnO_x/Ag NPs. Scale bars: 10 nm. **e** Schematic representation of catalytic mechanism of SnO_x/Ag. **f** FEs for SnO_x/Ag catalyst at different potentials. Free energy diagrams of CO_2 reduction to **g** HCOOH on SnO_2 (110) and SnO_2/Ag (111) and **h** CO on Ag (111) and SnO_2/Ag (111). Reprinted with permission from Ref. [155]. **i** Schematic representation of CO_2 to CO on the Ag and MO_x/Ag catalysts. FEs of H_2 and CO on **j** Ag NPs and **k** MnO_2/Ag NPs. Reprinted with permission from Ref. [160]

Different from conventional core–shell structure, the SnO_x/Ag heterostructure simultaneously possesses the exposed Ag and SnO_x sites, leading to dual function (Fig. 5e). As shown in Fig. 5f, CO and HCOOH are main productions in the more positive and negative potential range, respectively. In addition, it demonstrated much lower overpotential and higher FE of CO, and higher selectivity for HCOOH generation, compared with single-component Ag and SnO_x NPs, respectively. Importantly, the selective conversion of CO_2 to different products in different potential ranges can be achieved at the metal–oxide interface. Notably, the SnO_x/Ag heterostructure can avoid CO poisoning and thus present excellent catalytic stability that outperformed Pd, the only known material that can realize switch of HCOOH and CO at different potentials [156, 157]. The theoretical calculations accompanied with comparative experiment were carried out to study the internal mechanism. For the CO formation process, *COOH species are suggested to be more thermodynamically stable on the Ag sites, which can contribute to the additional O-Sn bond from SnO_2 sites. As for HCOOH, the existence of Ag sites weakens the binding of *OCHO on neighboring SnO_2 sites, which is conducive to HCOOH desorption. Furthermore, as shown in Fig. 5g, h, lower energy barrier for CO pathway serves as the main driving factor for CO-producing mode; at higher overpotential, more energetically favorable ΔG for the formation of *OCHO leads to HCOOH-producing mode. Besides, it is harder to adsorb H atoms for more positively charged Ag, contributed by the electron transfer from Ag to SnO_x in the whole potential range.

Inspired by other works [99, 119, 131, 158, 159], Yuan et al. systemically studied Ag-based catalyst with different Ag–metal oxide interfaces, i.e., MO_x/Ag (111) (M = Cu, Cr, Sn, Bi, Pb, Mn) [160]. As shown in Fig. 5i, MO_x/Ag interface can lower ΔG for the formation of *COOH and the key *COOH intermediate can be stabilized via additional coordination bonds between carbonyl and M at the interface. Meanwhile, the energy barrier for H_2 generation is increased

and thus HER is significantly suppressed. Figure 5j, k shows that MnO_2/Ag catalyst exhibits much higher FE of CO at more positive potential range (from − 0.5 to − 0.9 V vs. RHE) than pure Ag NPs. Notably, the FE of CO is up to 98.0% at − 0.7 V versus RHE, and the stability was increased considerably. Apart from these five metals, Mg and Ti oxides have also been investigated via DFT study and the Ag–oxide interface exhibits significant facilitation effect on CO_2 electroreduction [161, 162]. For the 2D MgO/Ag catalyst, the excellent electrocatalytic performance could be attributed to exotic surface states of MgO overlayers, mediated by electron coupling between MgO and Ag substrates. While for $(TiO_2)_3$/Ag(110) electrocatalyst, the Ti oxides/Ag interface functions by providing active sites for the adsorption and activation of CO_2 molecule. To be specific, Ag as electron donor could supply electrons to both $(TiO_2)_3$ and the absorbed CO_2, forming CO_2* at the interface.

3.3 Metal–Nonmetal Interface

Constructing metal–nonmetal interface is another strategy to improve CO_2RR efficiencies of metal catalysts [91]. The electron transfer from metal to nonmetal [163–167] triggered by the difference in electronegativity and the atomic level distance at the interface can contribute to the key steps in CO_2RR. In addition, the metal–nonmetal interface can be further modulated with various nonmetal elements, such as N, to tune the interfacial electron transfer.

For example, Wang et al. constructed N-doped nanodiamonds/Cu (N-ND/Cu) interface via sputtering Cu NPs on the surface of N-ND (Fig. 6a) [164], which exhibited one of the highest FE of C_2 products reported [62, 168–176]. As shown in Fig. 6b, compared with sole parent catalytic component, N-ND/Cu catalyzes CO_2 reduction in a more positive potential range (− 0.4 to − 0.7 V vs. RHE) and

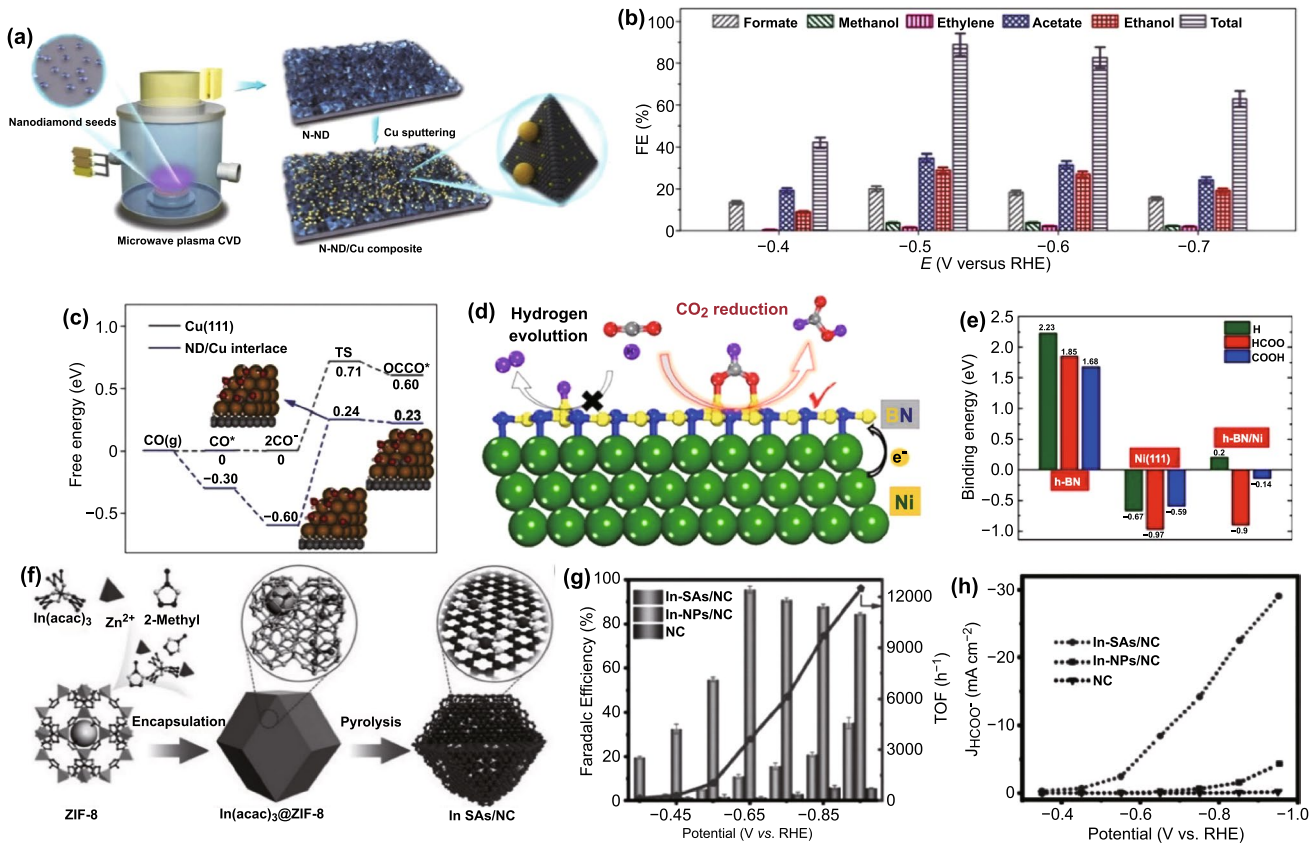

Fig. 6 **a** Schematic illustration for N-ND/Cu composite materials. **b** FEs of different products for N-ND/Cu catalyst. **c** ΔG diagram for CO coupling at the Cu and ND/Cu interface. Reprinted with permission from Ref. [164]. **d** Schematic diagram for CO_2RR at h-BN/Ni interface. **e** Binding energies of H, HCOO, and COOH on three catalysts. Reprinted with permission from Ref. [165]. **f** Schematic diagram for synthesis of In-SAs/NC. **g** FEs and TOF of $HCOO^-$ and **h** current densities for three catalysts. Reprinted with permission from Ref. [166]

https://doi.org/10.1007/s40820-021-00738-9

possesses higher activity and selectivity for acetate and ethanol. More importantly, the Cu mass activity as well as the unprecedented persistent catalytic performance up to 120 h at − 0.5 V versus RHE was achieved. According to double-layer capacitance measurements [177–179] and other analysis (grazing-incidence wide-angle X-ray scattering, SEM, etc.), the good durability is ascribed to the synergistic stabilization of N-ND/Cu interface. DFT calculations were carried out to reveal the possible intrinsic mechanism to shed light on the high activity and selectivity. Different from other reports [180, 181], they concluded that the charge transfer from Cu to diamond that results from subsurface O can strengthens CO binding at the interface which can further be facilitated by N doping. Therefore, as illustrated in Fig. 6c, the desorption of CO was suppressed and the dimerization of CO to *OCCO was enhanced, which is dynamically more favorable at the interface. In addition, the role of N doping can not only improve the conductivity of ND and the stability of Cu, but also lower energy barrier for formate generation with high selectivity.

Beside electronic effect, geometrical structure is also of vital importance [165, 182]. The h-BN monolayers were coupled with transition metals to develop CO_2RR electrocatalysts. Furthermore, DFT has been employed to investigate of the origin of activity of h-BN/metal for CO_2RR [165] through establishing the relationship between the optimized geometries and the different intermediates (such as H, HCOO, and COOH). As illustrated in Fig. 6d, the abundant electrons transfer from the metal to h-BN should predominate the conversion of CO_2 to HCOOH while HER is suppressed. Moreover, Fig. 6e clearly shows that at the h-BN/Ni interface, the binding energy of H and COOH is greatly weaken, while the change in HCOO binding is slight.

Over the past decade, more attention has been focused on single-atom catalyst due to its appealing electrocatalytic performance as a result of almost 100% atomic utilization [183–189]. However, a recent research showed that metal cluster catalyst with the atomic interface outperforms the corresponding single-atom catalysts [190], implying that the well-defined atomic interface can deliver outstanding catalytic performance. Very recently, the indium (In) single-atom catalyst with N-doped carbon matrix (In-SAs/NC) was prepared via a wet-impregnation process and subsequent a pyrolysis process, which possessed exclusive $In^{\delta+}$-N_4 atomic interface on MOFs derived N-doped carbon matrix (Fig. 6f) [166]. Compared with In nanoparticle catalyst (In-NPs/NC) and NC, Fig. 6g, h shows prominent enhancement on FE and current density of formate when In-SAs/NC was employed as catalyst, which was also well explained by DFT calculations. Notably, the FE and the current density of formate are up to 96% and 8.87 mA cm^{-2} at − 0.65 V versus RHE, respectively. Furthermore, the strategy can also be extended to other two group metals (Sn and Sb), and relevant single-atom catalyst both demonstrated excellent catalytic performance. The obtained Sn-SAs/NC and Sb-SAs/NC catalysts showed the maximum FE of 88% toward $HCOO^-$ at 0.75 V versus RHE and above FE of 80% in broad potential windows (− 0.65 to − 0.95 V vs. RHE), respectively. That is, they provided a new strategy with universality to construct main group metal single-atom catalysts with outstanding electrocatalytic performance for CO_2RR.

3.4 Metal Oxide–Metal Oxide Interface

According to previous works, the interface of metal oxide and metal oxide can enhance the adsorption and activation of CO_2 and the stabilization of CO_2^- intermediate on the surface of catalysts [191–194]. In addition, this electronic effect can also contribute to the formation and stabilization of active oxidation state species at the metal oxide–metal oxide interface [120, 195, 196]. Especially, strong electron transport or charge redistribution is highlighted, such as in Sn oxides [193, 194]. For example, electron transfer at SnO_2/Sn_3O_4 interface was investigated by Wu and co-workers [194]. SnO_2/Sn_3O_4 interface was obtained via a facial hydrothermal process and the as-obtained catalyst demonstrated apparent enhancement of CO_2RR (Fig. 7a, b). Both the current density and FE of formate for SnO_2/Sn_3O_4 catalyst are higher than those of single-component catalysts (Fig. 7c, d). Note that the highest FE of formate is up to 88.3% at − 0.9 V versus RHE. The experimental and theoretical results suggest that the excellent CO_2RR activity and selectivity should come from a built-in electric field at heterophase interface. More, the built-in electric field can reform electronic structure for CO_2 adsorption and HCOO* formation and facilitate electron transfer leading to fast reaction kinetics. It is the strong charge redistribution at interface that favors to keep Sn^{II} species (active for HCOOH) abundant and stable. More details about electron transport were studied about SnO_2/Bi_2O_3 interface later [193]. The electron transfer from Bi_2O_3 to SnO_2 endows SnO_2 with rich electron and prevents itself

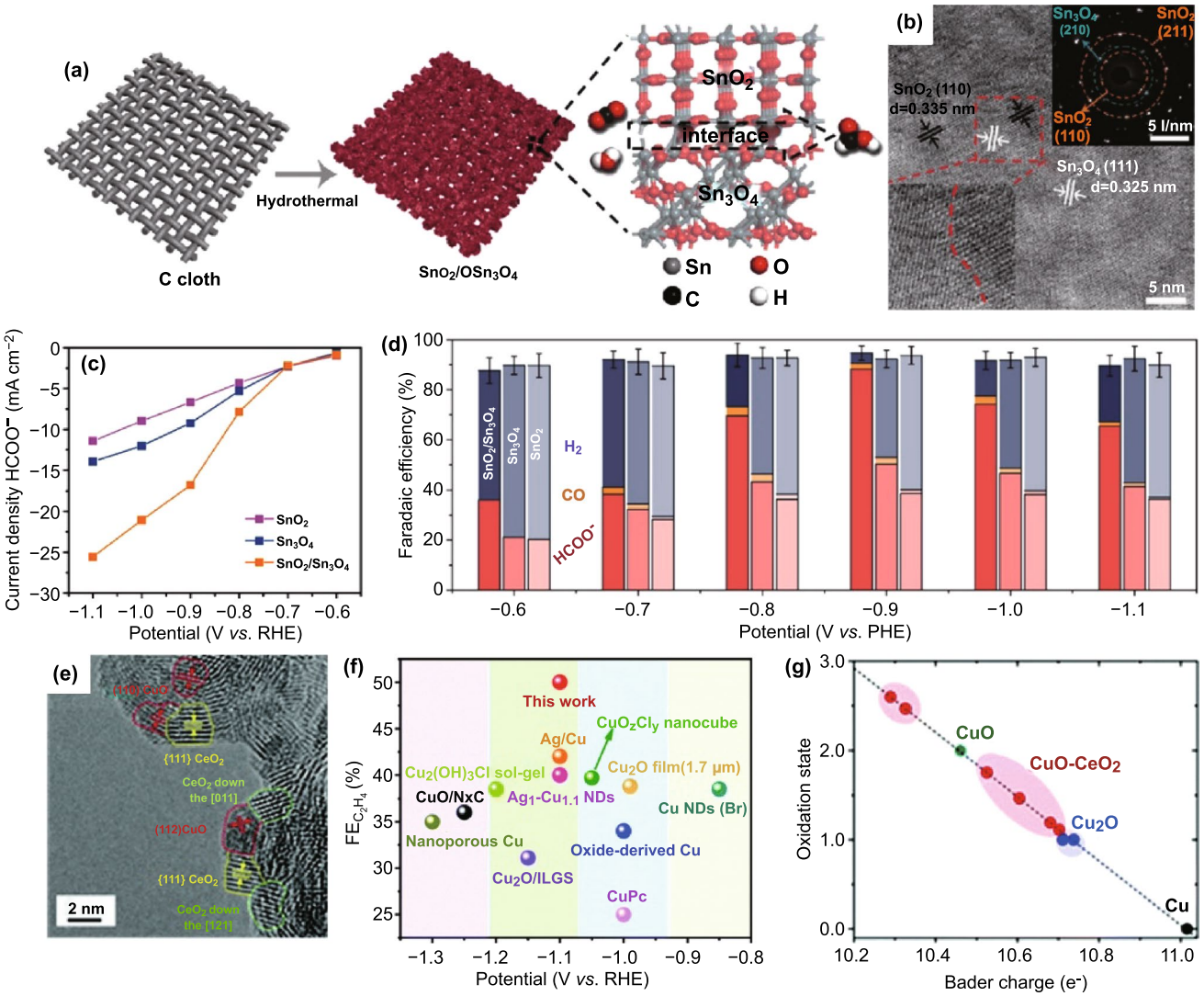

Fig. 7 **a** Schematic illustration of the synthetic process for the heterophase SnO_2/Sn_3O_4 nanosheets. **b** HRTEM image of SnO_2/Sn_3O_4. The inset is selected area electron diffraction pattern. **c** Partial current densities of HCOOH and **d** FEs of HCOOH, CO, and H_2 for SnO_2/Sn_3O_4, SnO_2 and Sn_3O_4. Reprinted with permission from Ref. [194]. **e** HRTEM image of CuO–CeO_2. **f** FEs of C_2H_4 for CuO-CeO_2 catalyst and other reported Cu-based electrocatalysts. **g** Bader charge analysis about oxidation states of surface Cu atoms. Reprinted with permission from Ref. [197]

from reduction for excellent durability. In addition, the introduced Bi_2O_3 can help to absorb HCOO* and convert reactant molecules to $HCOO^-$.

In addition, studies about the interface of CuO with other metal oxides, especially with CeO_2, have been reported. For example, Cu-based catalyst with abundant CuO/CeO_2 interfaces (Fig. 7e) was obtained regardless of mismatched lattices [197], which can catalyze CO_2 to ethylene with extremely high FE of 50.0% at − 1.1 V versus RHE, outperforming many recently reported Cu-based materials (Fig. 7f). Figure 7g shows that CeO_2 can change the oxidation state of Cu^{2+}(CuO) to Cu^+ which is crucial for reduction of CO_2 to C_{2+} products [198, 199]. In this case, CeO_2 severs as impetus for water activation in CO_2 reduction, which is kinetically in favor of the formation of *CHO and further formation of C_{2+} [200]. As for insight into how CeO_2 stabilizes the crucial Cu^+ species, i.e., specific electron transfer, it still needs to be further explored.

https://doi.org/10.1007/s40820-021-00738-9

3.5 Organic Molecules–Inorganic Materials Interface

Herein, the CO_2RR catalysts of organic molecule-modified inorganic materials are defined as surface coordination chemistry involved nanocomposite structures. This structure investigates how the type and the coordination of ligands influence catalytic activity of the inorganic materials at the molecular level. The surface ligand can not only lead to shape-controlled synthesis, but also trigger many fantastic surface properties of inorganic materials. Appropriate surface coordination chemistry has been reported to provide steric interactions and electronic modifications to the inorganic materials for promoting the catalytic activity. The current difficulty in the investigation of organic molecule-modified inorganic materials lies in the lack of appropriate and effective testing tools to visualize the molecular surface coordination structures. Generally speaking, the molecular mechanisms in surface coordination chemistry can be summarized in two important impacts of surface ligands effect and support effect. Specifically, the role of organic molecules in the study of CO_2RR can be summarized in the following four categories (Fig. 8): (i) modification of the electronic structure of inorganic materials, (ii) stabilization of the key reaction intermediates, (iii) regulation of mass diffusion (proton/CO_2), and (iv) modulation of the structural transformation.

3.5.1 Organic Molecule-Modified Cu

It is well known that Cu is one of the few metals that can reduce CO_2 to C_{2+} hydrocarbon products. However, the low selectivity of Cu is currently the main challenge for producing economically desirable hydrocarbons with high selectivity. The local environment has been proved to be very important in electrocatalysis through modulating the interactions among reactants or intermediates. Different strategies have been developed to optimize the Cu catalysts through morphology control, grain boundaries design, facets tuning, oxidation state modulation, and dopant manipulation. The above methods have demonstrated favorable and desirable reaction pathway by tuning the stabilities of intermediates for improving selectivity. Unfortunately, the FE of ethylene for Cu catalysts is still unsatisfactory with a low energy efficiency. Recently, the research developed a molecular tuning strategy in which N-arylpyridinium-derived film was used to functionalize the surface of Cu-based electrocatalysts

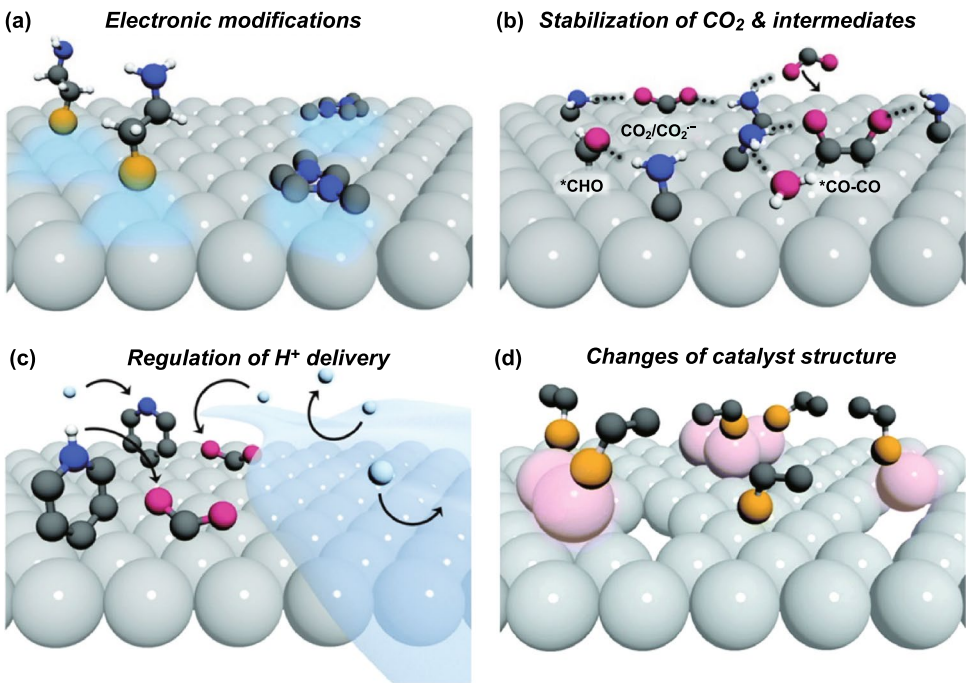

Fig. 8 Schematic illustration of the potential roles of organic molecules in modifying the activity and selectivity of inorganic materials for CO_2RR. Reprinted with permission from Ref. [201]

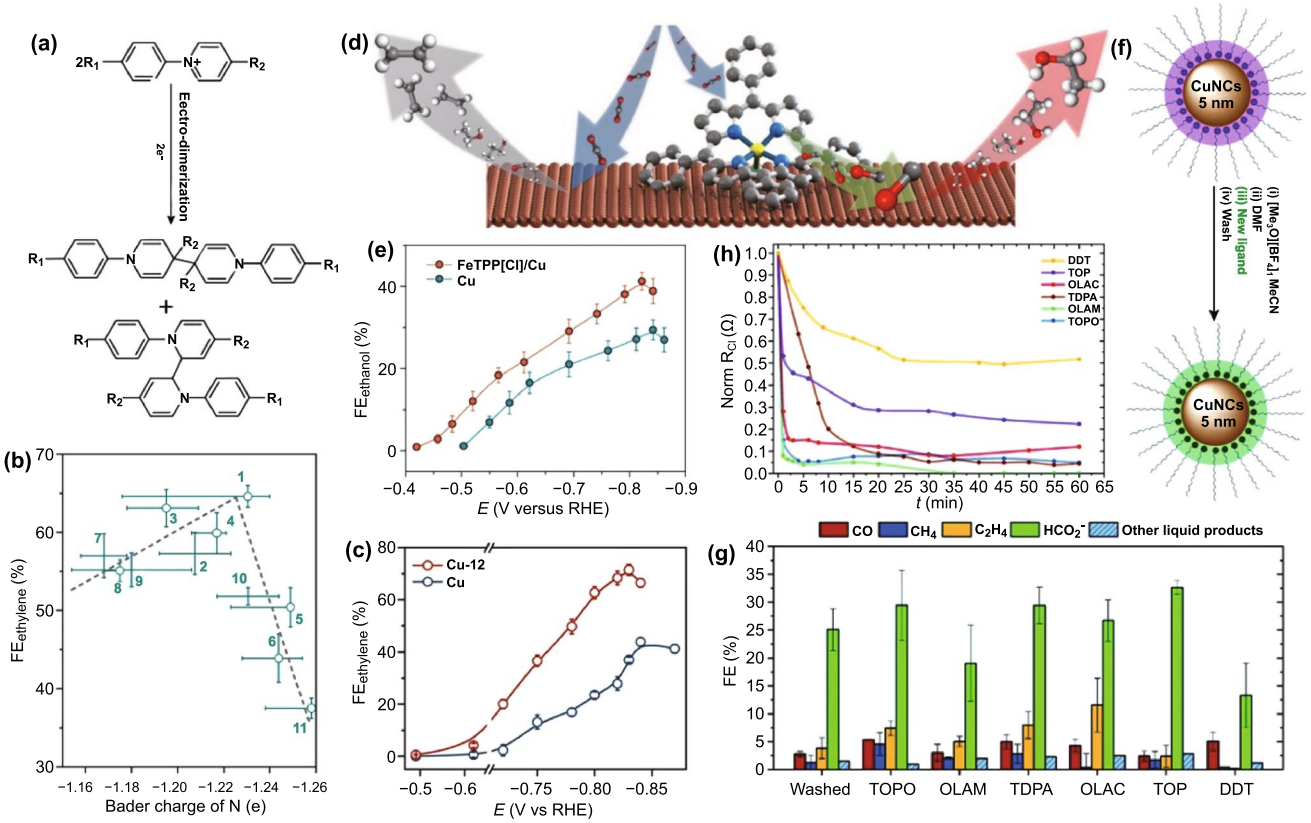

Fig. 9 **a** The process of converting N-arylpyridinium salt to mixture of N-aryl-substituted tetrahydro-bipyridines. **b** Relationship of FE of ethylene and calculated Bader charge for the nitrogen atom of the N-aryl-substituted tetrahydro-bipyridines. **c** FEs of ethylene on Cu and Cu-12. (12: *N*,*N*′-(1,4-phenylene) bispyridinium salt). Reprinted with permission from Ref. [202]. **d** Schematic illustration of molecular complexes on the Cu surface. **e** FEs of ethanol for the FeTPP[Cl]/Cu and Cu catalysts. Reprinted with permission from Ref. [203]. **f** Overview of preparing the CuNC catalysts with different ligands. **g** FEs of different reduction products. **h** Changes in the charge-transfer resistance (R_{CT}) over time for CuNCs capped by different ligands. Reprinted with permission from Ref. [204]

(Fig. 9a) [202]. Moreover, different types of molecules arising from electro-dimerization of arylpyridiniums have been investigated through systematic electrochemical test, operando/in situ spectroscopic study, and computational work. The Bader charge result signified a volcano-shaped trend relationship with FE of C_2H_4 (Fig. 9b), and the tetrahydrobipyridine that has suitable electron-donating ability showed a highest selectivity to C_2H_4. The result verified that the presence of organic molecules film on the surface of Cu can stabilize an 'atop-bound' CO intermediate, thereby leading to a high ethylene generation with a high FE of 72% (Fig. 9c), a high full-cell energy efficiency of 20%, and a good stability of 190 h. In addition, the molecule–metal catalyst interface was also cooperatively designed in order to generate local environment with rich reaction intermediates. Specifically, the Cu surface was functionalized with a library of porphyrin-based metallic complexes (Fig. 9d) [203]. Note that the adsorbed metallic complexes can catalyze the conversion of CO_2 to CO molecules. Aided by in situ/operando characterizations of Raman and X-ray absorption spectroscopies together with density functional theory calculations, it was verified that the surface metallic complexes can induce a high local concentration of CO intermediates, which can manipulate the C–C coupling through the ethanol pathway. The resultant FE for the conversion of CO_2 to ethanol is 41% (Fig. 9e), and the overall energy efficiency is 13%. The synthesis of colloidal nanoparticles inevitably requires organic ligands to control the size and morphology of the nanostructures. In this way, the structure–activity relationships of the catalysts can be well identified. However, the dynamic evolution of catalyst surface ligands in electrocatalysis and their role in the catalytic process are still

 https://doi.org/10.1007/s40820-021-00738-9

unclear. The research used Cu nanoparticle as benchmark catalysts to investigate the effects of capped different organic ligands (Fig. 9f) (i.e., oleylamine (OLAM), oleic acid (OLAC), dodecanethiol (DDT), trioctylphosphine (TOP), trioctylphosphine oxide (TOPO), and tetradecylphosphonic acid (TDPA)) on the CO_2RR activity [204]. The selection of ligands is based on the following three reasons, i.e., wide range of applications, varied binding strength derived from different functional groups, and a typical research case for studying the correlations between catalytic activity and ligand surface coverage. At the reaction potential, DDT can behave as a stable ligand on the surface of Cu, while TOPO, OLAM, TDPA, and OLAC are labile and will not affect the final selectivity and the activity of catalysts (Fig. 9g). TOP functions as a watershed to judge whether the ligand is stable (Fig. 9h). The stability of the surface ligands is binding-strength-related, which is dependent on the applied cathodic potential during electrocatalysis rather than their pristine electroreduction potentials. Based on the in situ observation, only the strongly bound ligands can produce a modulation for the electrocatalytic performance, while the weakly bound ligands were removed quickly at a relatively high cathodic potential. Therefore, aiming at the effective interface design between organic molecule and inorganic material, the research provided a criterion to choose persisted ligands.

3.5.2 *Organic Molecule-Modified Au*

Furthermore, a molecular of N-heterocyclic (NHC) carbene was used to modify the surface of Au nanoparticle for CO_2RR (Fig. 10a) [205]. Compared with the pristine Au nanoparticles with a FE of 53% toward CO, the designed catalyst showed a higher FE of 83% at the 0.46 V overpotential (Fig. 10b) with testing condition of neutral pH in water. With current density as an evaluation criterion, the modified Au exhibited about 7.6-fold increase, and meanwhile the NHC

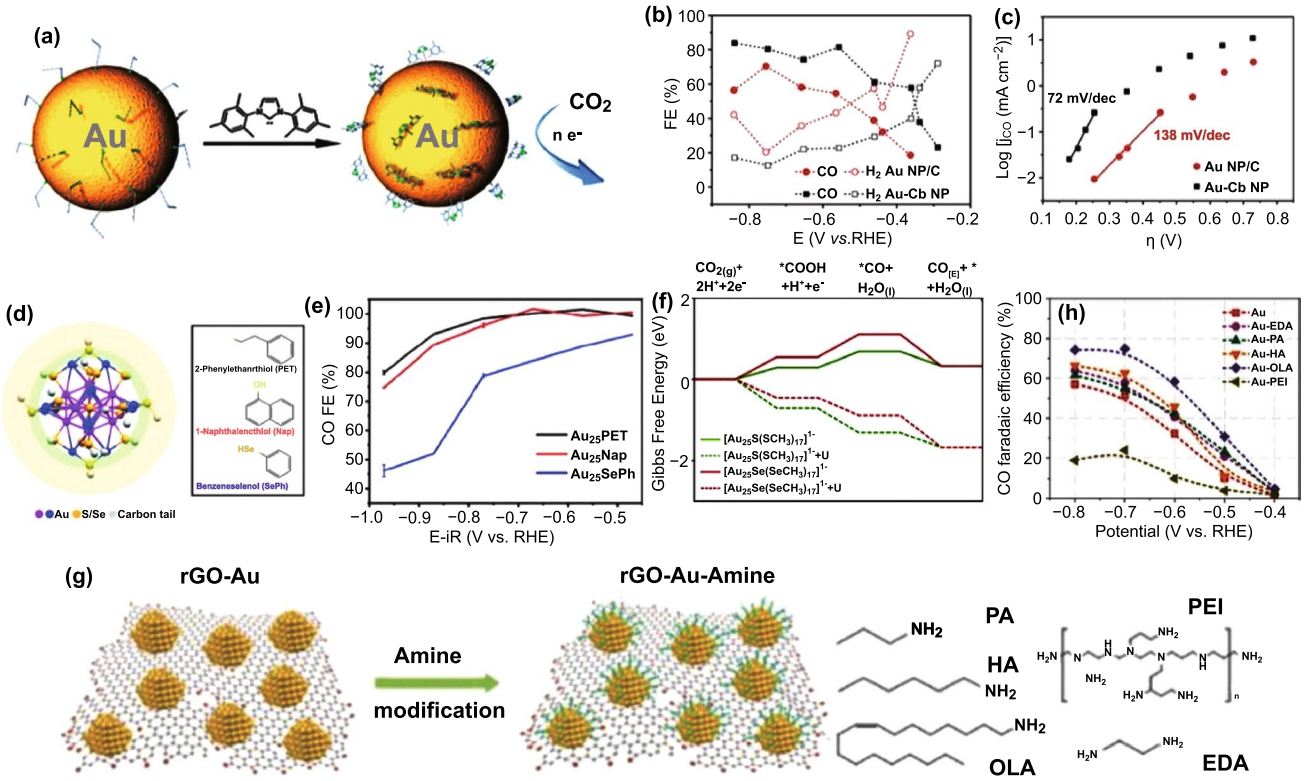

Fig. 10 **a** Schematic illustration of preparation and catalysis process of N-heterocyclic (NHC) carbene-functionalized Au NP catalyst. **b** FEs of CO and H_2 for Au–Cb NP and Au NP/C. **c** Tafel plots of Au–Cb NP and Au NP/C. Reprinted with permission from Ref. [205]. **d** Atom packing structures of Au_{25} and formulas of three ligands. **e** FEs of CO for Au_{25} nanoclusters. **f** Energetics of the CO_2RR pathway. Reprinted with permission from Ref. [206]. **g** Schematic illustration of amine modification on the rGO-Au composite. **h** FEs of CO for rGO-Au and Au-amine catalysts. Reprinted with permission from Ref. [124]

carbene-functionalized sample demonstrated a lower Tafel plot (72 mV/decade) than that of bare sample (138 mV/decade) (Fig. 10c). In addition to the strategies of size, shape, composition, and defect control for CO_2RR catalyst design, the molecular ligand approach can also effectively manipulate the mechanistic pathways toward higher performance.

Ligand effects have also been studied in the case of Au_{25} nanoclusters at the atomic level for CO_2RR [206]. The protecting ligand are varying from carbon tail to anchoring atom (S or Se) (Fig. 10d). The former (carbon tail) has no visible effect on the resultant catalytic activity and selectivity. In contrast, the latter (anchoring atom) exhibits significant effect on catalytic selectivity. Specifically, the anchoring atom Se tends to accelerate HER, while S can provide a high selectivity to CO (Fig. 10e). The theoretical calculation demonstrated that the energy barriers on S sites for the *COOH/*CO intermediate formations are about 0.26/0.43 eV lower than those of Se, respectively (Fig. 10f). The sulfur sites featured with higher electron density are suggested to be responsible for the bonding difference of the reaction intermediates. Therefore, the anchoring atoms at the metal–ligand interface are required to draw attention in the study of CO_2RR.

Ultrasmall Au nanoparticles typically have two contradictory properties, namely an abundance of low coordination sites in favor of HER and a high mass activity in favor of CO_2RR. In order to promote the CO_2RR efficiency, the ultrasmall Au nanoparticles with a size of 2.4 nm are loaded on reduced graphene oxide (Fig. 10g) [124]. The prepared catalyst exhibited FEs ranging from 32 to 60% (at overpotentials of 450–600 mV) and a high Au-specific mass activity of > 100 A g^{-1} for the conversion of CO_2 to CO. Interestingly, amine functionalized Au showed an obviously improved efficiencies to 59–75% and the high mass activities are still remained (Fig. 10h). Moreover, the activities of amine-Au catalysts for CO formation are highly dependent on the molecular structure of amine. The branched polyamine is verified to inhibit the CO generation. On the contrary, the linear amines, especially with high alkyl chain length, are beneficial to the formation of CO. The coverage of molecular involving metal–organics interaction and the molecular configuration may contribute to the CO_2RR.

The organic ligand capped Au showed a significant impact on the metal–oxide interactions (Au/SnO_2) for CO_2RR [158]. With cetyltrimethylammonium bromide (CTAB) as capping ligand, the Au endows the interface of Au/SnO_2 with CO generation at more positive potential and $HCOO^-$ formation at more negative potential, respectively (Fig. 11a). In contrast, when Au is capped with citrate, the Au/SnO_2 catalyst showed a high electivity to H_2 production among all potential (Fig. 11b). It indicated that the capping ligand can also modulate the metal–oxide interface for CO_2RR.

Three thiol-tethered ligands (2-mercaptopropionic acid, 4-pyridinylethanemercaptan, and cysteamine) functionalized Au nanoparticles were prepared to demonstrate the relationship between functional ligands and the CO_2RR selectivity (Fig. 11c–e) [207]. Compared with the pristine Au foil, the FE and the formate production of Au electrode capped with 4-pyridinylethanemercaptan delivered approximately two and threefold enhancement, respectively. Both promotion in CO and H_2 production was observed in cysteamine-modified Au electrode. The 2-mercaptopropionic-capped Au electrode exhibited almost 100% FE of H_2. The difference of the three types of ligands in pK_a is proposed to lead to varied proton-involved desorption mechanism, thus responsible for the dramatic change in the CO_2RR selectivity.

Moreover, molecularly defined interface (MDI) between Au and tetrakis-5,10,15,20-(4-aminophenyl) porphyrin (H_2TAPP) was constructed by precisely tuning the voltammetry cycle times in electrochemical oxidation deposition [208, 209]. The abundant Au site and amino functional group at the interface exhibited superior catalytic performance for CO_2RR (Fig. 11f) with CO selectivity of 95% at a potential of -0.7 V versus RHE (Fig. 11g). The catalytic performance is verified to be molecular layer thickness-dependent (Fig. 11h). Specifically, with the growing of the thickness of TAPP-PPN, the number of active sites at the MDI increases while the CO_2 diffusion pathways are blocked. The two inverse trends come to equilibrium when the thickness is 60 nm, which is signified to be beneficial to CO_2 diffusion kinetics.

A hybrid organic–inorganic catalyst of macrocycle cucurbit[6]uril (CB[6]) (Fig. 11i)-modified Au was developed to the control over the formation and the stabilization of reaction intermediates through engineering surface active sites of Au (Fig. 11j) [210]. The hydrophobic cavity of CB[6] is verified by surface-enhanced infrared absorption (SEIRA) spectroscopic experiment to increase the local CO_2 concentration close to the surface of Au in the testing condition of $KHCO_3$ aqueous solution. The experimental results of the difference in current densities of CO and H_2 generation indicated that the interaction form of intermediates inside

 https://doi.org/10.1007/s40820-021-00738-9

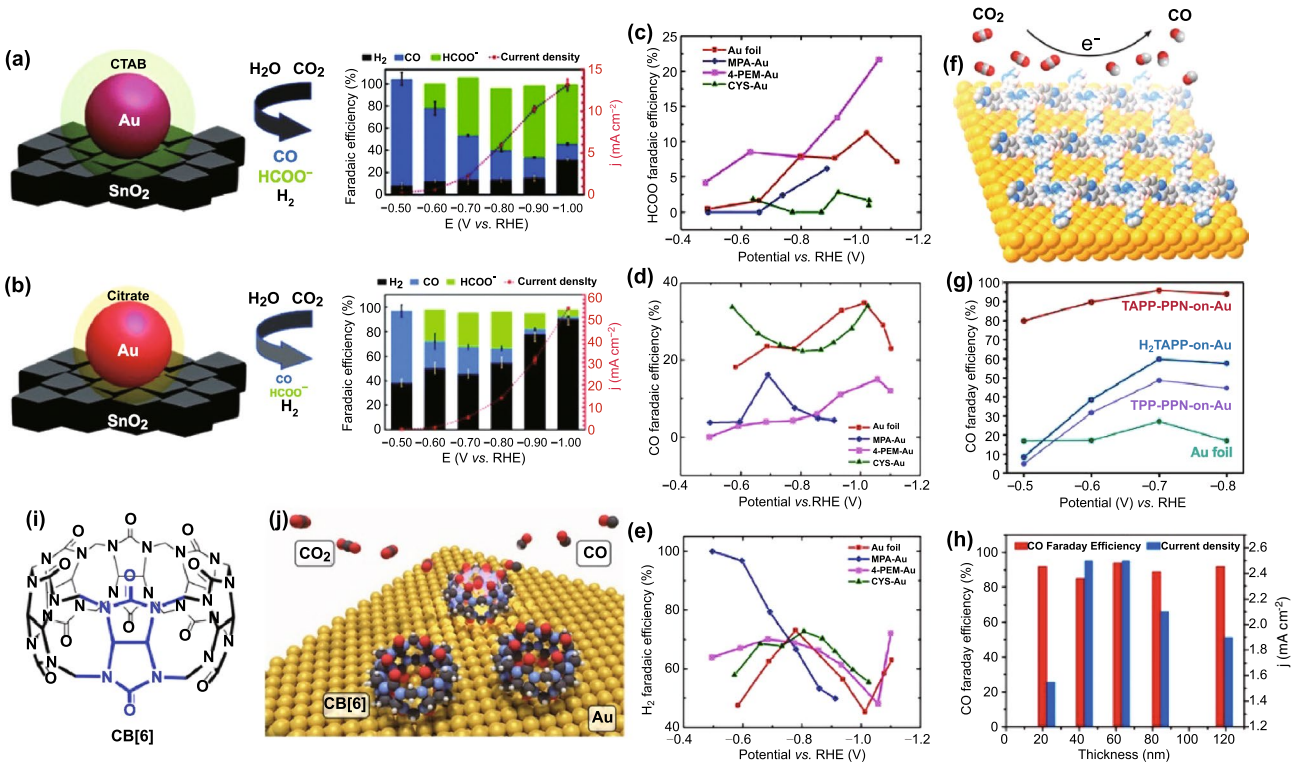

Fig. 11 Schematic illustration and catalytic performance of **a** CTAB-Au/SnO_2 and **b** Cit-Au/SnO_2 for the electroreduction of CO_2. Reprinted with permission from Ref. [158]. **c–e** FEs of $HCOO^-$, CO, and H_2 for three thiol-tethered ligands functionalized Au nanoparticles. Reprinted with permission from Ref. [207]. **f** Schematic illustration of catalysts with MDI. **g** FEs of CO for TAPP-PPN-60-on-Au, TTP-PPN-on-Au, H_2TAPP-on-Au, and Au foil. **h** FEs of CO and total current density of TAPP-PPN-on-Au related to the thickness at − 0.7 V versus RHE. Reprinted with permission from Ref. [208]. **i** The structure of CB[6]. **j** Schematic illustration of CO_2 conversion to CO within the cavity of CB[6] adsorbed on Au surface. Reprinted with permission from Ref. [210]

and outside the cavity is different, thereby suggesting an important methodology and mechanistic insight for organic molecule-modified inorganic materials to steer the reaction intermediates through interfacial host–guest chemistry.

3.5.3 Organic Molecule-Modified Ag

Electronic effects at the interface between Ag nanoparticles and Al-PMOF ([$Al_2(OH)_2$-(TCPP)]) (tetrakis (4-carboxyphenyl) porphyrin (TCPP)) were studied [211]. In this research, the native ligands on the surface of Ag were removed by the wrapping of MOF, thus providing an intimate contact at the Ag and MOF interface (Fig. 12a). The H_2 generation was drastically inhibited while the CO production was promoted in comparison with the pure Ag nanoparticles (Fig. 12b). Furthermore, the combination of MOF with Ag can obviously increase the stability of metal. The electron transfer from the Al-PMOF to the Ag nanoparticles, i.e., electronic effects, is suggested to be responsible for the selectivity promotion in CO_2RR, while the porous MOF layer-induced mass transport effects contribute a little to the promotion in the activity of CO_2RR.

3.6 Electrode and Electrolyte Interface

Although there has been considerable progress in CO_2RR, the understanding about the interface between the electrode and electrolyte remains poor and requires further efforts to elucidate many details, including ionic distribution, pH changes, the kinetics as well as the reaction barriers [201, 212, 213]. When involving solid–solution interface, it is perhaps easier to visualize an electric double layer at the interface of electrode and electrolyte, which is central to electrochemistry and governing external observations of electrochemical reactions.

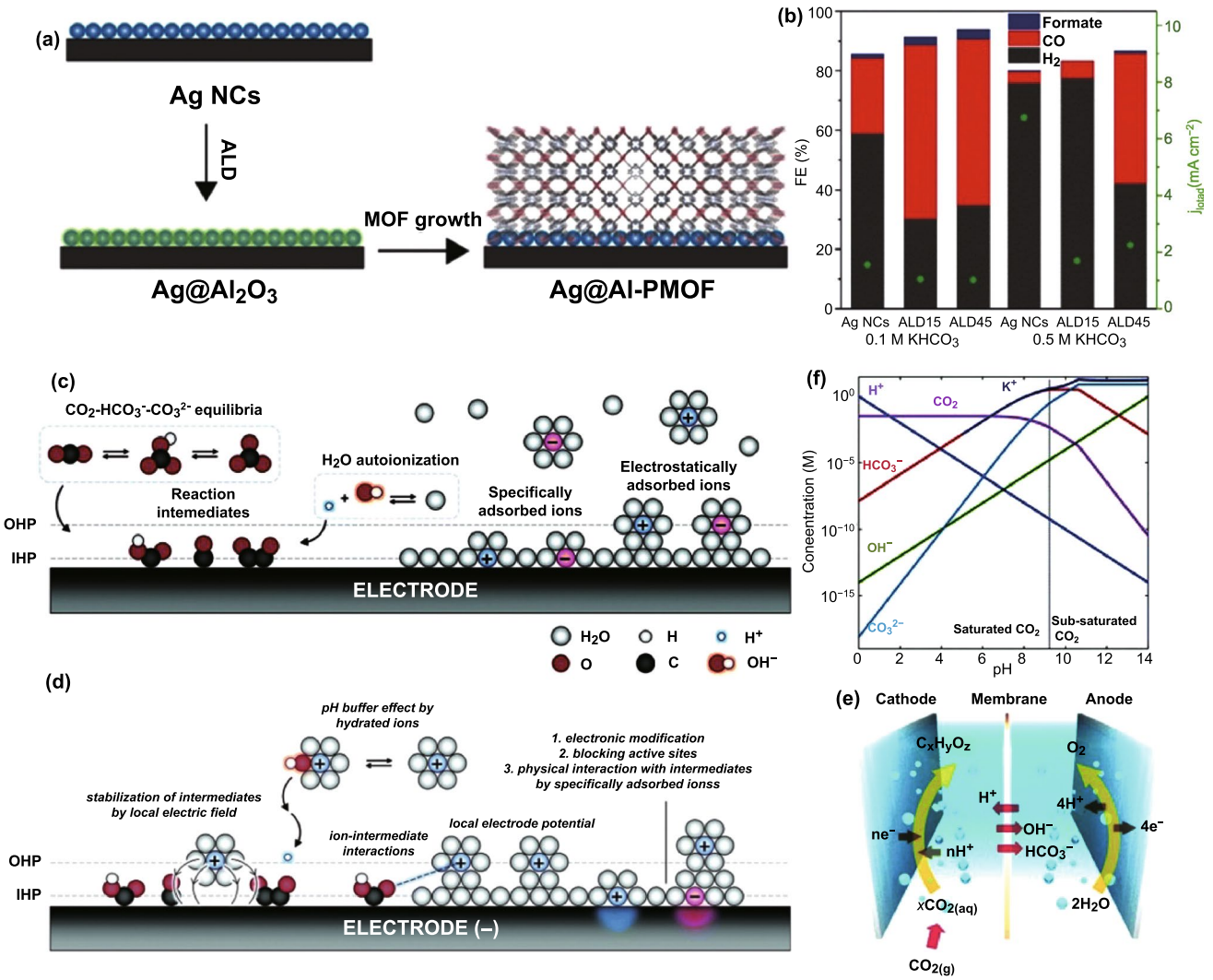

Fig. 12 **a** Scheme illustrating the synthesis of Ag@Al-PMOF hybrids. **b** FEs and total current densities for Ag NC and Ag@Al-PMOF catalysts. Reprinted with permission from Ref. [211]. **c** Schematic illustration of the electric double layer composed of IHP and OHP with chemical equilibria involved. **d** Schematic illustration of possible effects of the interfacial ions on the catalyst surface or the electrocatalytic process under the CO_2RR conditions with the negative potential applied. **e** Schematic illustration of the H-type cell for CO_2RR. Reprinted with permission from Ref. [201]. **f** Concentration of CO_2, H_2, OH^-, HCO_3^-, CO_3^{2-}, and K^+ as a function of bulk pH of the $KHCO_3/CO_3^{2-}$ electrolyte. Reprinted with permission from Ref. [214]

Typically, the reaction intermediates exist in the inner Helmholtz plane (IHP) by chemical bonding, while the hydrated ions lie in the outer Helmholtz plane (OHP) through electrostatic force (Fig. 12c, d). The type and number of ions and the pH (Fig. 12e, f) of the electrolyte can potentially affect the dynamic equilibria of H_2O and CO_2 at the interface [201, 214]. As a result, the different ions adsorbed on the surface of electrode can modulate the resultant CO_2RR process through multiple potential ways, such as interacting with the reaction intermediates, changing the morphological or electronic structure of the top surface of electrode, shielding some specific sites, and so on. However, at present, compared with the well-understood role of heterogeneous catalysts, the impact of electrolytes during CO_2RR always has been proposed only relying on the observed experimental performance and the simulation results [123], which has been suffering from insufficient understanding. The adequate characterization techniques are highly desired to drive forward the understanding about the role of electrolyte by monitoring the interactions of mass

 https://doi.org/10.1007/s40820-021-00738-9

diffusion and chemical balancing at the interface of electrode and electrolyte.

3.6.1 *Effects of Cation Size in Bicarbonate Electrolyte*

Bicarbonate is widely used as electrolyte for CO_2RR because it can not only offer near-neutral pH but also increase dissolved CO_2 concentration [215–219]. The size of cation in bicarbonate electrolyte has been verified to alter the activity and the selectivity in CO_2RR (Fig. 13a, b) by the relatively high aggregation of cations at the OHP due to cathodic reaction with negative potential [220–222]. The different views about the role of cation size are summarized as below: (i) The large cations are suggested to have relatively small hydration numbers in comparison with small ones, which has a tendency to be readily adsorbed on the electrode [220]. (ii) The cations at the OHP could upgrade the local potential, which are demonstrated to inhibit HER process by decreasing the local proton concentration [223]. The large cations could induce an increased interfacial dipole field in comparison with the small ones, which may stabilize the critical reaction intermediates (e.g., $*CO_2$, *CO, and *OCCO) with high dipole torque for producing formate, C_2H_4, and C_2H_5OH. (iii) The interfacial pH is suggested to be cation-size-dependent by in situ ATR-SEIRAS monitoring the interfacial concentration ratio of CO_2 and HCO_3^- [218, 224–226]. The pK_a value of large-size Cs^+ is evaluated to be about three times lower than that of small-size Li^+. Compared to Li^+, Cs^+ can function as a buffer and increase the local CO_2 concentration at the electrode–electrolyte interface by a factor of approximately 28 (Fig. 13c). As for the cations with different chemical valence, the cations with high valence but small size are suggested to deliver a significant impact for

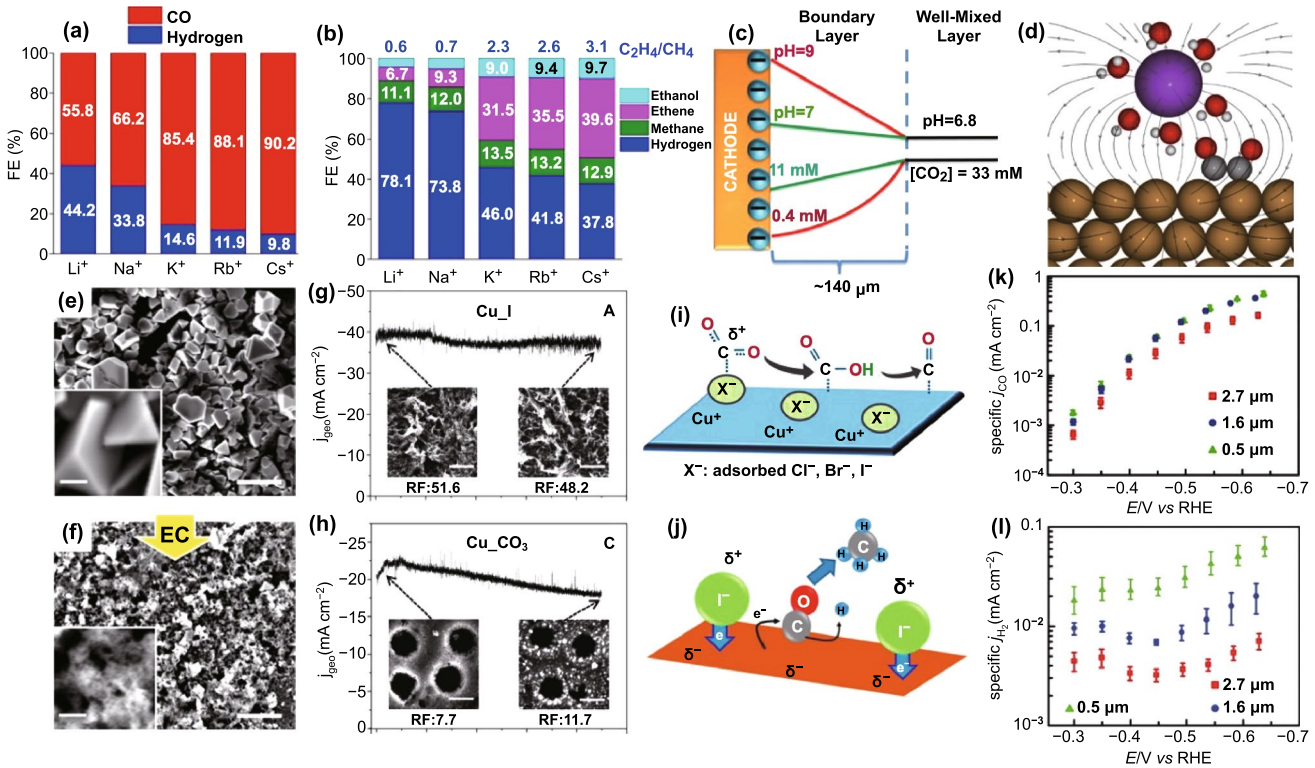

Fig. 13 **a** FEs of CO and H_2 for Ag. **b** FEs of C_2H_5OH, C_2H_4, CH_4, and H_2 for Cu. **c** Distribution of pH and CO_2 concentration in the boundary layer. Reprinted with permission from Ref. [225]. **d** Schematic illustration of the local electric field created by cation at the catalyst interface and stabilized OCCO intermediate. Reprinted with permission from Ref. [259] SEM images of Cu foils tested before **e** and after **f** the CO_2 electroreduction. Reprinted with permission from Ref. [233]. Time-dependent geometric current densities of gas products for **g** Cu_I and **h** Cu_CO_3 catalysts. Reprinted with permission from Ref. [235]. **i** Illustration of facilitation and stabilization of CO_2 adsorption and carboxyl intermediate, respectively. Reprinted with permission from Ref. [233]. **j** Illustration of how halide affects the net charge of Cu. Reprinted with permission from Ref. [232]. Current densities of **k** CO and **l** H_2. Reprinted with permission from Ref. [255]

the interfacial field (Fig. 13d) [223, 227, 259]. Note that the transition metal cation with even trace amount, such as Fe^{2+}, Zn^{2+}, etc., can trigger the deactivation of the working electrode by electrodeposition [228–230].

3.6.2 Effects of Anion Size

Despite the significant influence of cations, the role of the anions still cannot be ignored. The buffering capacity of the anions is thought to be an important factor in the regulation of CO_2RR pathways [231]. The selectivity to C_2 products involving C_2H_4 and C_2H_5OH is increased in non-buffering anions, such as SO_4^{2-} and ClO_4^-. Bicarbonate leads to a mixture of C_1 and C_2 products with moderate ratio. As for the phosphate, hydrogen is mainly produced at low overpotentials while CH_4 is dominant production at high overpotentials. Note that the formation of H_2 and CH_4 involves the proton transfers, while the other products, such CO, formate, C_2H_4, and C_2H_5OH, are independent of the proton supply. The research suggested that the buffering anion can function as a proton donor to modulate the pH altering, thereby promoting the selectivity to H_2 and CH_4. In contrast, non-buffering anion can result in an elevated OH^- concentration to inhibit the proton transfer, and as a result, the formation of H_2 and CH_4 was suppressed. Specifically, the anion halide in electrolyte is suggested to play multiple roles for CO_2RR: (i) The halide can trigger surface reconstruction involving the roughness altering and the exposure of active Cu (100) plane for C–C coupling reaction during electrochemical cycling or electroreduction (Fig. 13e, f) [232–236]. The surface electronic states of electrode are also proposed to be modulated by the strong interaction between the halide and the electrode (Fig. 13g, h). (ii) The halide can stabilize the Cu^+ species in Cu-based catalysts by forming Cu-halide composite that can stabilize methylene intermediate radicals thus favoring the formation of C–C bonds [168, 233]. It means that the binding energies of the reaction intermediates can be altered by the adsorption of halide on the surface of electrode. (iii) The halide can enhance the long-term stability (Fig. 13i, j) [235]. The selectivity of Cu-based electrodes to CH_4, C_2H_4, formate, and C_2H_5OH was reported to be increased in the presence of halide [232–234]. In addition, the effects of halide on the activity of Ag and Zn have also been investigated for selective CO production [237–242]. The adsorption of CN^- and Cl^- on Au surface is demonstrated to give a higher current density than the pristine one for CO production [243]. The theoretical calculation result indicates that the *COOH intermediate can be well stabilized by the adsorbed CN^- and Cl^- species via van der Walls interaction. In contrast, the effect of electrolytes on nonmetallic catalysts has been less well reported, mainly because of the complexity (presumably electric double layer) near electrode/electrolyte interface. Based on the effects of different cations and anions on the boron-doped diamond for CO_2RR, the formate selectivity was obviously affected by the alkali metal cations and the halide anions, but the trends are different from that in metal electrode, which needs further investigated [244–246].

3.6.3 Modulation of Reactants Supply

Moreover, beyond the essential role of catalyst in CO_2RR, the mass transport of the reactants including proton, H_2O, and CO_2 molecules exhibits significant impact on the resultant catalytic activity. The reason should be ascribed to the fact that at ambient condition, i.e., one atom, neutral pH, and room temperature, the low aqueous CO_2 solubility of about 33 mM suppresses the mass diffusion of CO_2 [214, 247], thereby limiting the overall catalytic activity for CO_2RR. The straightforward strategy for improving CO_2RR activity and selectivity is increasing the gaseous CO_2 supply at the interface. A new-developed electrode configuration of three-phase interface, i.e., catalyst (solid)–electrolyte (liquid)–CO_2 (gas), can provide high-concentrated CO_2 leading to high CO_2 reduction rates. Recently, different types of electrode design, such as polyethylene polymer-modified Au [248], 1-octadecanthiol-coated Cu dendrite [249], and graphene-coated wrapped Sn [250], have been successfully developed, and they all delivered high current density and high FE for CO_2RR. As a result, the strategies that can decrease the local proton concentration at the electrode–electrolyte interface are of significance to suppress the competitive parallel HER, thereby promoting CO_2RR activity and selectivity [251–254]. The well-tuned morphologies of electrode are suggested to induce local changes of pH at

https://doi.org/10.1007/s40820-021-00738-9

the electrode–electrolyte interface. The inverse opal structure of Au with increased thickness can result in a higher surface basicity to suppress partial current density of HER by about tenfold (Fig. 13k) with slight change in FE of CO (Fig. 13l) [255]. The morphology-dependent local pH change can also be demonstrated in the cases of Au and Zn catalysts [256, 257]. The result indicates that the modifications in the catalyst structures can modulate the supply of reactants (i.e., CO_2, H^+, and H_2O) at the electrode–electrolyte interface [258].

3.7 Molecular Catalysts–Electrode Interface

Some important molecular catalysts have been summarized in our recent reviews [73, 260, 261], herein we mainly report the latest findings. Compared with the extensively studied nanocrystal and single-atom catalysts, single-unit-cell catalysts existing as a bridge between the above two catalysts have rarely been reported because of the difficulties lying in synthesis and quantum effects. Recently, by introducing polyoxometalate (POM) cluster, Cu_9S_5 single-unit-cell with

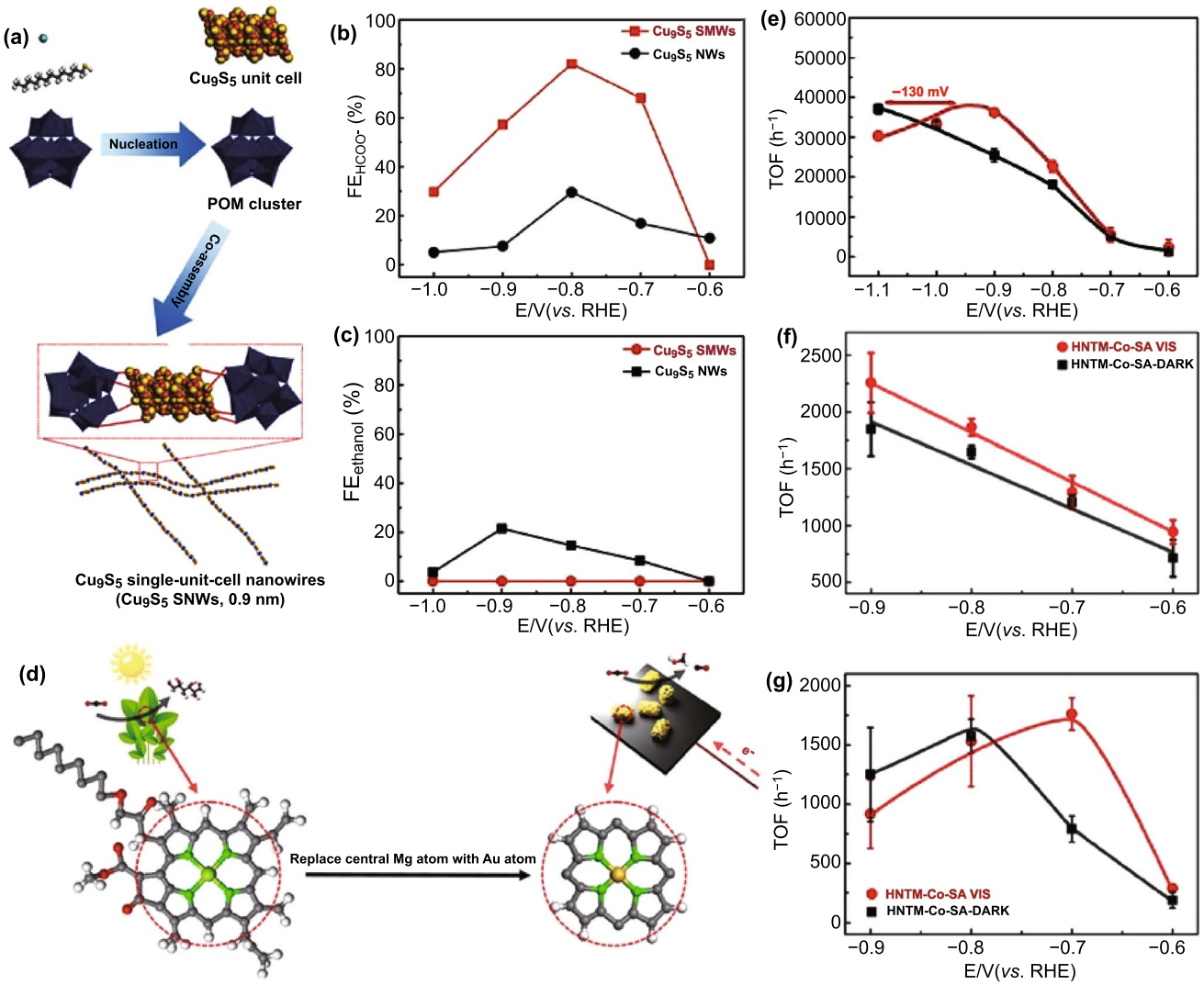

Fig. 14 **a** Schematic illustration of preparation of Cu_9S_5 SNWs. **b** FEs of $HCOO^-$ and **c** FEs of ethanol for Cu_9S_5 SNWs and Cu_9S_5 NWs. Reprinted with permission from Ref. [262]. **d** Schematic illustration of photosynthesis and photoelectrochemical reduction of CO_2 on chlorophyll and HNTM-Au-SA. TOF curves of **e** HNTM-Au-S, **f** HNTM-Co-SA and **g** HNTM-Cu-SA under visible light/dark. Reprinted with permission from Ref. [263]

sub-nanometer of 0.9 nm was prepared through modulating the nucleation pathway (Fig. 14a) [262]. Thus, each unit Cu_9S_5 cell can be regarded as molecular catalyst functioning as an isolated active site for CO_2RR. Compared with the complex productions ($HCOO^-$, methanol, and ethanol) of nanocrystal structure, the unit Cu_9S_5 cell shows dramatically increased electrocatalytic activity and FE of HCOOH (82.0%) (Fig. 14b, c). The research inspired that the decreasing the size of inorganic nanostructure down to sub-nanometer can achieve great chances for precise catalysis.

Normally, porphyrin serves as a ligand for metal center. A series of porphyrin-Au/Co/Cu catalysts consisting of zirconium porphyrinic metal–organic framework (MOF) hollow nanotubes (HNTMs) as supports and anchored metal atoms were prepared via a solvothermal method and subsequent heat treatment. The porphyrin can mimic the role of chlorophyll as a photoswitch to modulate the electron transfer routes to the metal center (Fig. 14d) [263, 264]. As a result, the light external field can reduce the potential by 130, 20, and 100 mV, respectively, for porphyrin-Au/Co/Cu catalysts (Fig. 14e–g). In addition, organic molecule (such as amino acid)-modified Cu electrodes showed significant enhancement on selectively converting CO_2 to hydrocarbons [265].

4 Conclusion and Perspective

The interface engineering has been developed to be an effective strategy to construct high-performance catalysts toward CO_2RR. In this review, we have summarized the fundamental and experimental progress in interface engineering for CO_2RR, which involves metal–metal, metal–metal oxide, metal–nonmetal, metal oxide–metal oxide, organic molecules–inorganic materials, electrode–electrolyte, and molecular catalysts–electrode interfaces, etc. Importantly, the electrocatalytic CO_2RR performance could be effectively modulated by interface engineering via electronic and/or structural modulation, regulations of electron/proton/mass/intermediates and the control of local reactant concentration, thereby achieving desirable reaction pathway, inhibiting competing hydrogen generation, breaking binding-energy scaling relations of intermediates, and promoting CO_2 mass transfer. Although great efforts have been devoted to the rational design and controlled fabrication of advanced catalysts with well-defined interfaces, the comprehensive and in-depth understanding of the interface–performance relationship in CO_2RR still remains a great challenge.

The construction of well-defined interfacial structures is very important to reveal their roles in the structure–performance relationship by the precise control of the interface at the atomic scale. The identification of refined interfacial structures usually requires a delicate combination of aberration-corrected TEM, XAFS analysis and appropriate theoretical simulation methods to confirm the coordination and bonding environment. Moreover, the CO_2RR involves the adsorption of CO_2 molecules, multi-electron and proton coupling process, C–C coupling process to generate multi-carbon products, interfacial active species migration or transfer process, and product desorption. The use of operando characterization techniques including but not limited to operando optical, X-ray, and electron-based techniques is highly desired to address some key issues about understanding the role of heterogeneous interface in the stability, the selectivity, and the reaction pathway under real operating conditions. The electrocatalytic tests serve as the dominant evidence to confirm the activity of interface structure. The establishment of accurate and reliable test methods and standards is very important to the development of the field of CO_2RR. Some pivotal experimental parameters and results, such as the configuration of electrochemical cell, the types of electrodes and electrolyte, the types of gas chromatography columns especially for detection of C_{2+} gas production and so on, should be well described. Theoretical calculations have advanced our understanding of the effect of interface on the CO_2RR process, and several new concepts and reaction pathways have been proposed. Theoretical calculations of the reaction process are suggested to combine the accurate interfacial structure and the detailed operando characterization, which is of great importance for the design of advanced CO_2RR catalysts, the revelation of reaction mechanism, etc. In addition, to obtain appreciable reaction rates and conversion efficiencies for CO_2RR, the electrocatalysis process are suggested to couple with the photo- and/or thermos energy. Thus, the interface should be designed to be active for the synergistic effect of different outer fields. In the near future, the breakthroughs in analysis techniques, data science and artificial intelligence are expected to bring revolutionary progress for the interface-related catalysis in CO_2RR.

Acknowledgements This work was supported by the National Natural Science Foundation of China (22071172), the

 https://doi.org/10.1007/s40820-021-00738-9

Ministry of Science and Technology of China (2016YFB0401100, 2017YFA0204503, and 2018YFA0703200), and Shandong Provincial Natural Science Foundation (No. ZR2019BB025).

References

1. P. Intasian, K. Prakinee, A. Phintha, D. Trisrivirat, N. Weeranoppanant et al., Enzymes, in vivo biocatalysis, and metabolic engineering for enabling a circular economy and sustainability. Chem. Rev. (2021). https://doi.org/10.1021/acs.chemrev.1c00121
2. S.Z. Xu, E.A. Carter, Theoretical insights into heterogeneous (photo)electrochemical CO_2 reduction. Chem. Rev. **119**(11), 6631–6669 (2019). https://doi.org/10.1021/acs.chemrev.8b00481
3. L. Weiss, W. Ludwig, S. Heussner, M. Canals, J.F. Ghiglione et al., The missing ocean plastic sink: gone with the rivers. Science **373**(6550), 107–111 (2021). https://doi.org/10.1126/science.abe0290
4. D.J. Beerling, E.P. Kantzas, M.R. Lomas, P. Wade, R.M. Eufrasio et al., Potential for large-scale CO_2 removal via enhanced rock weathering with croplands. Nature **583**, 242–248 (2020). https://doi.org/10.1038/s41586-020-2448-9
5. A. Chen, B.L. Lin, A simple framework for quantifying electrochemical CO_2 fixation. Joule **2**(4), 594–606 (2018). https://doi.org/10.1016/j.joule.2018.02.003
6. E.V. Kondratenko, G. Mul, J. Baltrusaitis, G.O. Larrazábal, J. Pérez-Ramírez, Status and perspectives of CO_2 conversion into fuels and chemicals by catalytic, photocatalytic and electrocatalytic processes. Energy Environ. Sci. **6**, 3112–3135 (2013). https://doi.org/10.1039/C3EE41272E
7. A. Vasileff, Y. Zheng, S. Qiao, Carbon solving carbon's problems: recent progress of nanostructured carbon-based catalysts for the electrochemical reduction of CO_2. Adv. Energy Mater. **7**(21), 1700759 (2017). https://doi.org/10.1002/aenm.201700759
8. W. Bi, X. Li, R. You, M. Chen, R. Yuan et al., Surface immobilization of transition metal ions on nitrogen-doped graphene realizing high-efficient and selective CO_2 reduction. Adv. Mater. **30**(18), 1706617 (2018). https://doi.org/10.1002/adma.201706617
9. W. Zhang, Y. Hu, L. Ma, G. Zhu, Y. Wang et al., Progress and perspective of electrocatalytic CO_2 reduction for renewable carbonaceous fuels and chemicals. Adv. Sci. **5**(1), 1700275 (2018). https://doi.org/10.1002/advs.201700275
10. Q. Lu, J. Rosen, Y. Zhou, G.S. Hutchings, Y.C. Kimmel et al., A selective and efficient electrocatalyst for carbon dioxide reduction. Nat. Commun. **5**, 3242 (2014). https://doi.org/10.1038/ncomms4242
11. D. Zhu, J. Liu, S. Qiao, Recent advances in inorganic heterogeneous electrocatalysts for reduction of carbon dioxide. Adv. Mater. **28**(18), 3423–3452 (2016). https://doi.org/10.1002/adma.201504766
12. E.E. Benson, C.P. Kubiak, A.J. Sathrum, J.M. Smieja, Electrocatalytic and homogeneous approaches to conversion of CO_2 to liquid fuels. Chem. Soc. Rev. **38**(1), 89–99 (2009). https://doi.org/10.1039/B804323J
13. K. Khan, A.K. Tareen, M. Aslam, R.U.R. Sagar, B. Zhang et al., Recent progress, challenges, and prospects in two-dimensional photo-catalyst materials and environmental remediation. Nano-Micro Lett. **12**, 167 (2020). https://doi.org/10.1007/s40820-020-00504-3
14. E. Dlugokencky, P. Tans, NOAA/ESRL, http://www.esrl.noaa.gov/gmd/ccgg/trends/. Accessed July 2021
15. J.G. Canadell, C. Le Quere, M.R. Raupach, C.B. Field, E.T. Buitenhuis et al., Contributions to accelerating atmospheric CO_2 growth from economic activity, carbon intensity, and efficiency of natural sinks. Proc. Natl. Acad. Sci. USA **104**(47), 18866–18870 (2007). https://doi.org/10.1073/pnas.0702737104
16. M. Mikkelsen, M. Jørgensen, F.C. Krebs, The teraton challenge. A review of fixation and transformation of carbon dioxide. Energy Environ. Sci. **3**, 43–81 (2010). https://doi.org/10.1039/B912904A
17. M.R. Raupach, G. Marland, P. Ciais, C. Le Quéré, J.G. Canadell et al., Global and regional drivers of accelerating CO_2 emissions. Proc. Natl. Acad. Sci. USA **104**(24), 10288–10293 (2007). https://doi.org/10.1073/pnas.0700609104
18. S. Gao, Z. Sun, W. Liu, X. Jiao, X. Zu et al., Atomic layer confined vacancies for atomic-level insights into carbon dioxide electroreduction. Nat. Commun. **8**, 14503 (2017). https://doi.org/10.1038/ncomms14503
19. I. Ganesh, Conversion of carbon dioxide into methanol—a potential liquid fuel: fundamental challenges and opportunities (a review). Renew. Sustain. Energy Rev. **31**, 221–257 (2014). https://doi.org/10.1016/j.rser.2013.11.045
20. J. Zhong, X. Yang, Z. Wu, B. Liang, Y. Huang et al., State of the art and perspectives in heterogeneous catalysis of CO_2 hydrogenation to methanol. Chem. Soc. Rev. **49**, 1385–1413 (2020). https://doi.org/10.1039/C9CS00614A
21. N.S. Lewis, D.G. Nocera, Powering the planet: chemical challenges in solar energy utilization. Proc. Natl. Acad. Sci. **103**(43), 15729–15735 (2006). https://doi.org/10.1073/pnas.0603395103

22. G. Centi, S. Perathoner, Opportunities and prospects in the chemical recycling of carbon dioxide to fuels. Catal. Today **148**(3–4), 191–205 (2009). https://doi.org/10.1016/j.cattod.2009.07.075
23. G.A. Olah, A. Goeppert, G.S. Prakash, Chemical recycling of carbon dioxide to methanol and dimethyl ether: from greenhouse gas to renewable, environmentally carbon neutral fuels and synthetic hydrocarbons. J. Org. Chem. **74**(2), 487–498 (2009). https://doi.org/10.1021/jo801260f
24. Z. Chen, K. Mou, X. Wang, L. Liu, Nitrogen-doped graphene quantum dots enhance the activity of Bi_2O_3 nanosheets for electrochemical reduction of CO_2 in a wide negative potential region. Angew. Chem. Int. Ed. **57**(39), 12790–12794 (2018). https://doi.org/10.1002/anie.201807643
25. N. Wang, R.K. Miao, G. Lee, A. Vomiero, D. Sinton et al., Suppressing the liquid product crossover in electrochemical CO_2 reduction. SmartMat **2**(1), 12–16 (2021). https://doi.org/10.1002/smm2.1018
26. T. Gao, A. Kumar, Z. Shang, X. Duan, H. Wang et al., Promoting electrochemical conversion of CO_2 to formate with rich oxygen vacancies in nanoporous tin oxides. Chin. Chem. Lett. **30**(12), 2274–2778 (2019). https://doi.org/10.1016/j.cclet.2019.07.028
27. M. Zhou, Y. Lin, H. Xia, X. Wei, Y. Yao et al., A molecular foaming and activation strategy to porous N-doped carbon foams for supercapacitors and CO_2 capture. Nano-Micro Lett. **12**, 58 (2020). https://doi.org/10.1007/s40820-020-0389-3
28. K. Mou, Z. Chen, X. Zhang, M. Jiao, X. Zhang et al., Highly efficient electroreduction of CO_2 on nickel single-atom catalysts: atom trapping and nitrogen anchorin. Small **15**(49), 1903668 (2019). https://doi.org/10.1002/smll.201903668
29. Q. Gong, P. Ding, M. Xu, X. Zhu, M. Wang et al., Double-slit photoelectron interference in strong-field ionization of the neon dimer. Nat. Commun. **10**, 1 (2019). https://doi.org/10.1038/s41467-018-07882-8
30. T. Zheng, K. Jiang, H. Wang, Recent advances in electrochemical CO_2-to-Co conversion on heterogeneous catalysts. Adv. Mater. **30**(48), 1802066 (2018). https://doi.org/10.1002/adma.201802066
31. L. Zhang, Z.J. Zhao, J. Gong, Nanostructured materials for heterogeneous electrocatalytic CO_2 reduction and their related reaction mechanisms. Angew. Chem. Int. Ed. **56**(38), 11326–11353 (2017). https://doi.org/10.1002/anie.201612214
32. C. Costentin, M. Robert, J.M. Savéant, Catalysis of the electrochemical reduction of carbon dioxide. Chem. Soc. Rev. **42**(6), 2423–2436 (2013). https://doi.org/10.1039/C2CS35360A
33. J. Qiao, Y. Liu, F. Hong, J. Zhang, A review of catalysts for the electroreduction of carbon dioxide to produce low-carbon fuels. Chem. Soc. Rev. **43**(2), 631–675 (2014). https://doi.org/10.1039/C3CS60323G
34. L. Zhang, Z. Zhao, T. Wang, J. Gong, Nano-designed semiconductors for electro- and photoelectro-catalytic conversion of carbon dioxide. Chem. Soc. Rev. **47**(14), 5423–5443 (2018). https://doi.org/10.1039/C8CS00016F
35. J. Albo, M. Alvarez-Guerra, P. Castaño, A. Irabien, Towards the electrochemical conversion of carbon dioxide into methanol. Green Chem. **17**(4), 2304–2324 (2015). https://doi.org/10.1039/C4GC02453B
36. P. De Luna, C. Hahn, D. Higgins, S.A. Jaffer, T.F. Jaramillo et al., What would it take for renewably powered electrosynthesis to displace petrochemical processes? Science **364**(6438), eaav3506 (2019). https://doi.org/10.1126/science.aav3506
37. Z. Chen, K. Mou, S. Yao, L. Liu, Zinc-coordinated nitrogen-codoped graphene as an efficient catalyst for selective electrochemical reduction of CO_2 to CO. ChemSusChem **11**(17), 2944–2952 (2018). https://doi.org/10.1002/cssc.201800925
38. X. Chang, T. Wang, J. Gong, CO_2 photo-reduction: insights into CO_2 activation and reaction on surfaces of photocatalysts. Energy Environ. Sci. **9**(7), 2177–2196 (2016). https://doi.org/10.1039/C6EE00383D
39. X. Chang, T. Wang, P. Zhang, Y. Wei, J. Zhao et al., Stable aqueous photoelectrochemical CO_2 reduction by a Cu_2O dark cathode with improved selectivity for carbonaceous products. Angew. Chem. Int. Ed. **55**(31), 8840–8845 (2016). https://doi.org/10.1002/anie.201602973
40. L. Liu, Y. Jiang, H. Zhao, J. Chen, J. Cheng et al., Engineering coexposed 001 and 101 facets in oxygen-deficient TiO_2 nanocrystals for enhanced CO_2 photoreduction under visible light. ACS Catal. **6**(2), 1097–1108 (2016). https://doi.org/10.1021/acscatal.5b02098
41. A.J. Morris, G.J. Meyer, E. Fujita, Molecular approaches to the photocatalytic reduction of carbon dioxide for solar fuels. Acc. Chem. Res. **42**(12), 1983–1994 (2009). https://doi.org/10.1021/ar9001679
42. S.C. Roy, O.K. Varghese, M. Paulose, C.A. Grimes, Toward solar fuels: photocatalytic conversion of carbon dioxide to hydrocarbons. ACS Nano **4**(3), 1259–1278 (2010). https://doi.org/10.1021/nn9015423
43. M. Schreier, J. Luo, P. Gao, T. Moehl, M.T. Mayer et al., Covalent immobilization of a molecular catalyst on Cu_2O photocathodes for CO_2 reduction. J. Am. Chem. Soc. **138**(6), 1938–1946 (2016). https://doi.org/10.1021/jacs.5b12157
44. S. Wang, X. Wang, Imidazolium ionic liquids, imidazolylidene heterocyclic carbenes, and zeolitic imidazolate frameworks for CO_2 capture and photochemical reduction. Angew. Chem. Int. Ed. **55**(7), 2308–2320 (2016). https://doi.org/10.1002/anie.201507145
45. J. Yu, J. Low, W. Xiao, P. Zhou, M. Jaroniec, Enhanced photocatalytic CO_2-reduction activity of anatase TiO_2 by coexposed 001 and 101 facets. J. Am. Chem. Soc. **136**(25), 8839–8842 (2014). https://doi.org/10.1021/ja5044787
46. X. Chen, X. Su, H. Su, X. Liu, S. Miao et al., Theoretical insights and the corresponding construction of supported metal catalysts for highly selective CO_2 to CO conversion. ACS Catal. **7**(7), 4613–4620 (2017). https://doi.org/10.1021/acscatal.7b00903
47. M. Mondal, S. Khanra, O. Tiwari, K. Gayen, G. Halder, Role of carbonic anhydrase on the way to biological carbon capture

 https://doi.org/10.1007/s40820-021-00738-9

through microalgae—a mini review. Environ. Prog. Sustain. **35**(6), 1605–1615 (2016). https://doi.org/10.1002/ep.12394

48. J. Shi, Y. Jiang, Z. Jiang, X. Wang, X. Wang et al., Enzymatic conversion of carbon dioxide. Chem. Soc. Rev. **44**(17), 5981–6000 (2015). https://doi.org/10.1039/C5CS00182J
49. W. Bao, H. Li, Y. Zhang, Selective leaching of steelmaking slag for indirect CO_2 mineral sequestration. Ind. Eng. Chem. Res. **49**(5), 2055–2063 (2010). https://doi.org/10.1021/ie801850s
50. J. Highfield, H. Lim, J. Fagerlund, R. Zevenhoven, Activation of serpentine for CO_2 mineralization by flux extraction of soluble magnesium salts using ammonium sulfate. RSC Adv. **2**(16), 6535–6541 (2012). https://doi.org/10.1039/C2RA01347A
51. J.W. Ko, S.W. Kim, J. Hong, J. Ryu, K. Kang et al., Synthesis of graphene-wrapped CuO hybrid materials by CO_2 mineralization. Green Chem. **14**(9), 2391–2394 (2012). https://doi.org/10.1039/C2GC35560D
52. C. Liu, J.J. Gallagher, K.K. Sakimoto, E.M. Nichols, C.J. Chang et al., Nanowire-bacteria hybrids for unassisted solar carbon dioxide fixation to value-added chemicals. Nano Lett. **15**(5), 3634–3639 (2015). https://doi.org/10.1021/acs.nanolett.5b01254
53. O. Martin, A.J. Martín, C. Mondelli, S. Mitchell, T.F. Segawa et al., Indium oxide as a superior catalyst for methanol synthesis by CO_2 hydrogenation. Angew. Chem. Int. Ed. **55**(21), 6261–6265 (2016). https://doi.org/10.1002/anie.201600943
54. F. Studt, I. Sharafutdinov, F. Abild-Pedersen, C.F. Elkjær, J.S. Hummelshøj et al., Discovery of a Ni–Ga catalyst for carbon dioxide reduction to methanol. Nat. Chem. **6**, 320–324 (2014). https://doi.org/10.1038/nchem.1873
55. Z. Gao, C. Wang, J. Li, Y. Zhu, Z. Zhang et al., Conductive metal–organic frameworks for electrocatalysis: achievements, challenges, and opportunities. Acta Phys-Chim. Sin. **37**(7), 2010025 (2020). https://doi.org/10.3866/PKU.WHXB202010025
56. K. Jiang, S. Siahrostami, T. Zheng, Y. Hu, S. Hwang et al., Isolated Ni single atoms in graphene nanosheets for high-performance CO_2 reduction. Energy Environ. Sci. **11**(4), 893–903 (2018). https://doi.org/10.1039/C7EE03245E
57. N. Han, Y. Wang, H. Yang, J. Deng, J. Wu et al., Ultrathin bismuth nanosheets from in situ topotactic transformation for selective electrocatalytic CO_2 reduction to formate. Nat. Commun. **9**, 1320 (2018). https://doi.org/10.1038/s41467-018-03712-z
58. L. Fu, R. Wang, C. Zhao, J. Huo, C. He et al., Construction of Cr-embedded graphyne electrocatalyst for highly selective reduction of CO_2 to CH_4: a DFT study. Chem. Eng. J. **414**, 128857 (2021). https://doi.org/10.1016/j.cej.2021.128857
59. J. Li, Y. Chen, Z. Fan, Z. Zhang, Editorial: Emerging technologies for materials design and characterization in energy conversion and storage. Front. Energy Res. **9**, 676876 (2021). https://doi.org/10.3389/fenrg.2021.676876
60. Z. Chen, K. Mou, S. Yao, L. Liu, Highly selective electrochemical reduction of CO_2 to formate on metal-free nitrogen-doped PC61BM. J. Mater. Chem. A **6**(24), 11236–11243 (2018). https://doi.org/10.1039/C8TA03328E
61. M. Gattrell, N. Gupta, A. Co, A review of the aqueous electrochemical reduction of CO_2 to hydrocarbons at copper. J. Electroanal. Chem. **594**(1), 1–19 (2006). https://doi.org/10.1016/j.jelechem.2006.05.013
62. K.P. Kuhl, E.R. Cave, D.N. Abram, T.F. Jaramillo, New insights into the electrochemical reduction of carbon dioxide on metallic copper surfaces. Energy Environ. Sci. **5**(5), 7050–7059 (2012). https://doi.org/10.1039/C2EE21234J
63. C.W. Li, M.W. Kanan, CO_2 reduction at low overpotential on cu electrodes resulting from the reduction of thick Cu_2O films. J. Am. Chem. Soc. **134**(17), 7231–7234 (2012). https://doi.org/10.1021/ja3010978
64. A.A. Peterson, F. Abild-Pedersen, How copper catalyzes the electroreduction of carbon dioxide into hydrocarbon fuels. Energy Environ. Sci. **3**(9), 1311–1315 (2010). https://doi.org/10.1039/C0EE00071J
65. C. Yang, F. Nosheen, Z. Zhang, Recent progress in structural modulation of metal nanomaterials for electrocatalytic CO_2 reduction. Rare Met. **40**, 1412–1430 (2020). https://doi.org/10.1007/s12598-020-01600-4
66. G. Centi, Smart catalytic materials for energy transition. SmartMat **1**(1), e1005 (2020). https://doi.org/10.1002/smm2.1005
67. J.H. Montoya, L.C. Seitz, P. Chakthranont, A. Vojvodic, T.F. Jaramillo et al., Materials for solar fuels and chemicals. Nat. Mater. **16**, 70–81 (2016). https://doi.org/10.1038/nmat4778
68. Z.W. Seh, J. Kibsgaard, C.F. Dickens, I. Chorkendorff, J.K. Norskov et al., Combining theory and experiment in electrocatalysis: insights into materials design. Science **355**(6321), eaad4998 (2017). https://doi.org/10.1126/science.aad4998
69. X. Zheng, P.D. Luna, F.P. García de Arquer, B. Zhang, N. Becknell et al., Sulfur-modulated tin sites enable highly selective electrochemical reduction of CO_2 to formate. Joule **1**(4), 794–805 (2017). https://doi.org/10.1016/j.joule.2017.09.014
70. Y. Matsubara, Standard electrode potentials for the reduction of CO_2 to CO in acetonitrile-water mixtures determined using a generalized method for proton-coupled electron-transfer reactions. ACS Energy Lett. **2**(8), 1886–1891 (2017). https://doi.org/10.1021/acsenergylett.7b00548
71. F. Li, S.F. Zhao, L. Chen, A. Khan, D.R. MacFarlane et al., Polyethylenimine promoted electrocatalytic reduction of CO_2 to CO in aqueous medium by graphene-supported amorphous molybdenum sulphide. Energy Environ. Sci. **9**(1), 216–223 (2016). https://doi.org/10.1039/C5EE02879E
72. Z. Sun, T. Ma, H. Tao, Q. Fan, B. Han, Fundamentals and challenges of electrochemical CO_2 reduction using two-dimensional materials. Chem **3**(4), 560–587 (2017). https://doi.org/10.1016/j.chempr.2017.09.009
73. C. Yang, S. Li, Z. Zhang, H. Wang, H. Liu et al., Organic–inorganic hybrid nanomaterials for electrocatalytic CO_2 reduction. Small **16**(29), 2001847 (2020). https://doi.org/10.1002/smll.202001847

74. Y. Liu, S. Chen, X. Quan, H. Yu, Efficient electrochemical reduction of carbon dioxide to acetate on nitrogen-doped nanodiamond. J. Am. Chem. Soc. **137**(36), 11631–11636 (2015). https://doi.org/10.1021/jacs.5b02975
75. S. Nitopi, E. Bertheussen, S.B. Scott, X. Liu, A.K. Engstfeld et al., Progress and perspectives of electrochemical CO_2 reduction on copper in aqueous electrolyte. Chem. Rev. **119**(12), 7610–7672 (2019). https://doi.org/10.1021/acs.chemrev.8b00705
76. X. Li, Z. Kou, J. Wang, Manipulating interfaces of electrocatalysts down to atomic scales: fundamentals, strategies, and electrocatalytic applications. Small Methods **5**(2), 2001010 (2020). https://doi.org/10.1002/smtd.202001010
77. Q. Shao, P. Wang, X. Huang, Opportunities and challenges of interface engineering in bimetallic nanostructure for enhanced electrocatalysis. Adv. Funct. Mater. **29**(8), 1806419 (2019). https://doi.org/10.1002/adfm.201806419
78. L. Wang, W. Chen, D. Zhang, Y. Du, R. Amal et al., Surface strategies for catalytic CO_2 reduction: from two-dimensional materials to nanoclusters to single atoms. Chem. Soc. Rev. **48**(21), 5310–5349 (2019). https://doi.org/10.1039/C9CS00163H
79. Y. Wang, P. Han, X. Lv, L. Zhang, G. Zheng, Defect and interface engineering for aqueous electrocatalytic CO_2 reduction. Joule **2**(12), 2551–2582 (2018). https://doi.org/10.1016/j.joule.2018.09.021
80. J. Zhong, X. Jin, L. Meng, X. Wang, H. Su et al., Probing the electronic and catalytic properties of a bimetallic surface with 3 nm resolution. Nat. Nanotechnol. **12**, 132–136 (2017). https://doi.org/10.1038/nnano.2016.241
81. L. Hou, J. Han, C. Wang, Y. Zhang, Y. Wang et al., Ag nanoparticle embedded Cu nanoporous hybrid arrays for the selective electrocatalytic reduction of CO_2 towards ethylene. Inorg. Chem. Front. **7**(10), 2097–2106 (2020). https://doi.org/10.1039/D0QI00025F
82. J. Wang, Z. Li, C. Dong, Y. Feng, J. Yang et al., Silver/copper interface for relay electroreduction of carbon dioxide to ethylene. ACS Appl. Mater. Interfaces **11**(3), 2763–2767 (2019). https://doi.org/10.1021/acsami.8b20545
83. J. Huang, M. Mensi, E. Oveisi, V. Mantella, R. Buonsanti, Structural sensitivities in bimetallic catalysts for electrochemical CO_2 reduction revealed by Ag–Cu nanodimers. J. Am. Chem. Soc. **141**(6), 2490–2499 (2019). https://doi.org/10.1021/jacs.8b12381
84. D. Zang, Q. Li, G. Dai, M. Zeng, Y. Huang et al., Interface engineering of Mo_8/Cu heterostructures toward highly selective electrochemical reduction of carbon dioxide into acetate. Appl. Catal. B-Environ. **281**, 119426 (2021). https://doi.org/10.1016/j.apcatb.2020.119426
85. Q. Li, M. Li, S. Zhang, X. Liu, X. Zhu et al., Tuning Sn–Cu catalysis for electrochemical reduction of CO_2 on partially reduced oxides SnO_x–CuO_x-modified Cu electrodes. Catalysts **9**(5), 476 (2019). https://doi.org/10.3390/catal9050476
86. T. Zhuang, Z. Liang, A. Seifitokaldani, Y. Li, P.D. Luna et al., Steering post-C–C coupling selectivity enables high efficiency electroreduction of carbon dioxide to multi-carbon alcohols. Nat. Catal. **1**, 421–428 (2018). https://doi.org/10.1038/s41929-018-0084-7
87. P.D. Luna, R. Quintero-Bermudez, C.T. Dinh, M.B. Ross, O.S. Bushuyev et al., Catalyst electro-redeposition controls morphology and oxidation state for selective carbon dioxide reduction. Nat. Catal. **1**, 103–110 (2018). https://doi.org/10.1038/s41929-017-0018-9
88. K. Jiang, R.B. Sandberg, A.J. Akey, X. Liu, D.C. Bell et al., Metal ion cycling of Cu foil for selective C–C coupling in electrochemical CO_2 reduction. Nat. Catal. **1**, 111–119 (2018). https://doi.org/10.1038/s41929-017-0009-x
89. Z. Weng, X. Zhang, Y. Wu, S. Huo, J. Jiang et al., Self-cleaning catalyst electrodes for stabilized CO_2 reduction to hydrocarbons. Angew. Chem. Int. Ed. **56**(42), 13135–13139 (2017). https://doi.org/10.1002/anie.201707478
90. X. Chang, T. Wang, Z. Zhao, P. Yang, J. Greeley et al., Tuning Cu/Cu_2O interfaces for the reduction of carbon dioxide to methanol in aqueous solutions. Angew. Chem. Int. Ed. **57**(47), 15415–15419 (2018). https://doi.org/10.1002/anie.201805256
91. L. Ye, M. Zhang, P. Huang, G. Guo, M. Hong et al., Enhancing CO_2 electrolysis through synergistic control of non-stoichiometry and doping to tune cathode surface structures. Nat. Commun. **8**, 14785 (2017). https://doi.org/10.1038/ncomms14785
92. M. Karamad, V. Tripkovic, J. Rossmeisl, Intermetallic alloys as CO electroreduction catalysts-role of isolated active sites. ACS Catal. **4**(7), 2268–2273 (2014). https://doi.org/10.1021/cs500328c
93. Y. Zhou, F. Che, M. Liu, C. Zou, Z. Liang et al., Author Correction: Dopant-induced electron localization drives CO_2 reduction to C_2 hydrocarbons. Nat. Chem. **11**, 1167 (2019). https://doi.org/10.1038/s41557-019-0381-z
94. J. Jiao, R. Lin, S. Liu, W.C. Cheong, C. Zhang et al., Copper atom-pair catalyst anchored on alloy nanowires for selective and efficient electrochemical reduction of CO_2. Nat. Chem. **11**, 222–228 (2019). https://doi.org/10.1038/s41557-018-0201-x
95. J. Xie, J. Chen, Y. Huang, X. Zhang, W. Wang et al., Selective electrochemical CO_2 reduction on Cu–Pd heterostructure. Appl. Catal. B-Environ. **270**, 118864 (2020). https://doi.org/10.1016/j.apcatb.2020.118864
96. H. Yang, Y. Hu, J. Chen, M.S. Balogun, P. Fang et al., Intermediates adsorption engineering of CO_2 electroreduction reaction in highly selective heterostructure Cu-based electrocatalysts for CO production. Adv. Energy Mater. **9**(27), 1901396 (2019). https://doi.org/10.1002/aenm.201901396
97. Z. Pan, E. Han, J. Zheng, J. Lu, X. Wang et al., Highly efficient photoelectrocatalytic reduction of CO_2 to methanol by a p–n heterojunction CeO_2/CuO/Cu catalyst. Nano-Micro Lett. **12**, 18 (2020). https://doi.org/10.1007/s40820-019-0354-1
98. S. Siahrostami, A. Verdaguer-Casadevall, M. Karamad, D. Deiana, P. Malacrida et al., Enabling direct H_2O_2 production through rational electrocatalyst design. Nat. Mater. **12**, 1137–1143 (2013). https://doi.org/10.1038/nmat3795

 https://doi.org/10.1007/s40820-021-00738-9

99. D. Kim, J. Resasco, Y. Yu, A.M. Asiri, P. Yang, Synergistic geometric and electronic effects for electrochemical reduction of carbon dioxide using gold–copper bimetallic nanoparticles. Nat. Commun. **5**, 4948 (2014). https://doi.org/10.1038/ncomms5948
100. C. Xia, Y. Zhou, C. He, A.I. Douka, W. Guo et al., Recent advances on electrospun nanomaterials for zinc-air batteries. Small Sci. **1**, 2100010 (2021). https://doi.org/10.1002/smsc.202100010
101. S. Back, J.H. Kim, Y.T. Kim, Y. Jung, Bifunctional interface of Au and Cu for improved CO_2 electroreduction. ACS Appl. Mater. Interfaces **8**(35), 23022–23027 (2016). https://doi.org/10.1021/acsami.6b05903
102. W. Luo, W. Xie, R. Mutschler, E. Oveisi, G.L. De Gregorio et al., Selective and stable electroreduction of CO_2 to CO at the copper/indium interface. ACS Catal. **8**(7), 6571–6581 (2018). https://doi.org/10.1021/acscatal.7b04457
103. C. Choi, J. Cai, C. Lee, H.M. Lee, M. Xu et al., Intimate atomic Cu–Ag interfaces for high CO_2RR selectivity towards CH_4 at low over potential. Nano Res. (2021). https://doi.org/10.1007/s12274-021-3639-x
104. C.G. Morales-Guio, E.R. Cave, S.A. Nitopi, J.T. Feaster, L. Wang et al., Improved CO_2 reduction activity towards C_{2+} alcohols on a tandem gold on copper electrocatalyst. Nat. Catal. **1**, 764–771 (2018). https://doi.org/10.1038/s41929-018-0139-9
105. E.L. Clark, C. Hahn, T.F. Jaramillo, A.T. Bell, Electrochemical CO_2 reduction over compressively strained CuAg surface alloys with enhanced multi-carbon oxygenate selectivity. J. Am. Chem. Soc. **139**(44), 15848–15857 (2017). https://doi.org/10.1021/jacs.7b08607
106. T.T.H. Hoang, S. Verma, S. Ma, T.T. Fister, J. Timoshenko et al., Nanoporous copper–silver alloys by additive-controlled electrodeposition for the selective electroreduction of CO_2 to ethylene and ethanol. J. Am. Chem. Soc. **140**(17), 5791–5797 (2018). https://doi.org/10.1021/jacs.8b01868
107. Q. Xiao, S.E. Sherman, S.E. Wilner, X. Zhou, C. Dazen et al., Janus dendrimersomes coassembled from fluorinated, hydrogenated, and hybrid Janus dendrimers as models for cell fusion and fission. Proc. Natl. Acad. Sci. USA **114**(34), E7045–E7053 (2017). https://doi.org/10.1073/pnas.1708380114
108. X. Bai, Q. Li, L. Shi, X. Niu, C. Ling et al., Hybrid Cu^0 and Cu^{x+} as atomic interfaces promote high-selectivity conversion of CO_2 to C_2H_5OH at low potential. Small **16**(12), 1901981 (2020). https://doi.org/10.1002/smll.201901981
109. R. Daiyan, W.H. Saputera, Q. Zhang, E. Lovell, S. Lim et al., 3D heterostructured copper electrode for conversion of carbon dioxide to alcohols at low overpotentials. Adv. Sustain. Syst. **3**(1), 1800064 (2019). https://doi.org/10.1002/adsu.201800064
110. M. Li, X. Tian, S. Garg, T.E. Rufford, P. Zhao et al., Modulated Sn oxidation states over a Cu_2O-derived substrate for selective electrochemical CO_2 reduction. ACS Appl. Mater. Interfaces **12**(20), 22760–22770 (2020). https://doi.org/10.1021/acsami.0c00412
111. L. Fan, Z. Xia, M. Xu, Y. Lu, Z. Li, 1D SnO_2 with wire-in-tube architectures for highly selective electrochemical reduction of CO_2 to C_1 products. Adv. Funct. Mater. **28**(17), 1706289 (2018). https://doi.org/10.1002/adfm.201706289
112. S. Zhao, S. Li, T. Guo, S. Zhang, J. Wang et al., Advances in Sn-based catalysts for electrochemical CO_2 reduction. Nano-Micro Lett. **11**, 62 (2019). https://doi.org/10.1007/s40820-019-0293-x
113. W. Lee, Y.E. Kim, M.H. Youn, S.K. Jeong, K.T. Park, Catholyte-free electrocatalytic CO_2 reduction to formate. Angew. Chem. Int. Ed. **57**(23), 6883–6887 (2018). https://doi.org/10.1002/anie.201803501
114. J. Gu, F. Heroguel, J. Luterbacher, X. Hu, Densely packed, ultra small SnO nanoparticles for enhanced activity and selectivity in electrochemical CO_2 reduction. Angew. Chem. Int. Ed. **57**(11), 2943–2947 (2018). https://doi.org/10.1002/anie.201713003
115. J. Zeng, K. Bejtka, W. Ju, M. Castellino, A. Chiodoni et al., Advanced Cu–Sn foam for selectively converting CO_2 to CO in aqueous solution. Appl. Catal. B-Environ. **236**(15), 475–482 (2018). https://doi.org/10.1016/j.apcatb.2018.05.056
116. S. Sarfraz, A.T. Garcia-Esparza, A. Jedidi, L. Cavallo et al., Cu–Sn bimetallic catalyst for selective aqueous electroreduction of CO_2 to CO. ACS Catal. **6**(5), 2842–2851 (2016). https://doi.org/10.1021/acscatal.6b00269
117. Y. Zhao, C. Wang, G.G. Wallace, Tin nanoparticles decorated copper oxide nanowires for selective electrochemical reduction of aqueous CO_2 to CO. J. Mater. Chem. A **4**(27), 10710–10718 (2016). https://doi.org/10.1039/C6TA04155H
118. J.T. Feaster, C. Shi, E.R. Cave, T. Hatsukade, D.N. Abram et al., Understanding selectivity for the electrochemical reduction of carbon dioxide to formic acid and carbon monoxide on metal electrodes. ACS Catal. **7**(7), 4822–4827 (2017). https://doi.org/10.1021/acscatal.7b00687
119. Q. Li, J. Fu, W. Zhu, Z. Chen, B. Shen et al., Tuning Sn-catalysis for electrochemical reduction of CO_2 to CO via the core/shell Cu/SnO_2 structure. J. Am. Chem. Soc. **139**(12), 4290–4293 (2017). https://doi.org/10.1021/jacs.7b00261
120. X. An, S. Li, A. Yoshida, Z. Wang, X. Hao et al., Electrodeposition of Tin-based electrocatalysts with different surface tin species distributions for electrochemical reduction of CO_2 to HCOOH. ACS Sustain. Chem. Eng. **7**(10), 9360–9368 (2019). https://doi.org/10.1021/acssuschemeng.9b00515
121. J.H. Kim, H. Woo, J. Choi, H.W. Jung, Y.T. Kim, CO_2 electroreduction on Au/TiC: enhanced activity due to metal–support interaction. ACS Catal. **7**(3), 2101–2106 (2017). https://doi.org/10.1021/acscatal.6b03706
122. X. Shen, X. Liu, S. Wang, T. Chen, W. Zhang et al., Synergistic modulation at atomically dispersed Fe/Au interface for selective CO_2 electroreduction. Nano Lett. **21**(1), 686–692 (2021). https://doi.org/10.1021/acs.nanolett.0c04291
123. M. Liu, Y. Pang, B. Zhang, P.D. Luna, O. Voznyy et al., Enhanced electrocatalytic CO_2 reduction via field-induced reagent concentration. Nature **537**, 382–386 (2016). https://doi.org/10.1038/nature19060

124. Y. Zhao, C. Wang, Y. Liu, D.R. MacFarlane, G.G. Wallace, Engineering surface amine modifiers of ultrasmall gold nanoparticles supported on reduced graphene oxide for improved electrochemical CO_2 reduction. Adv. Energy Mater. **8**(25), 1801400 (2018). https://doi.org/10.1002/aenm.201801400
125. W. Zheng, F. Chen, Q. Zeng, Z. Li, B. Yang et al., A universal principle to accurately synthesize atomically dispersed metal-N_4 sites for CO_2 electroreduction. Nano-Micro Lett. **12**, 108 (2020). https://doi.org/10.1007/s40820-020-00443-z
126. A.M. Ismail, G.F. Samu, H.C. Nguyen, E. Csapo, N. Lopez et al., Au/Pb interface allows the methane formation pathway in carbon dioxide electroreduction. ACS Catal. **10**(10), 5681–5690 (2020). https://doi.org/10.1021/acscatal.0c00749
127. Y. Chen, Z. Fan, J. Wang, C. Ling, W. Niu et al., Ethylene selectivity in electrocatalytic CO_2 reduction on Cu nanomaterials: a crystal phase-dependent study. J. Am. Chem. Soc. **142**(59), 12760–12766 (2020). https://doi.org/10.1021/jacs.0c04981
128. Y. Zhao, X. Liu, D. Chen, Z. Liu, Q. Yang et al., Atomic-level-designed copper atoms on hierarchically porous gold architectures for high-efficiency electrochemical CO_2 reduction. Sci. China Mater. **64**, 1900–1909 (2021). https://doi.org/10.1007/s40843-020-1583-4
129. X. Zhang, S. Feng, C. Zhan, D. Wu, Y. Zhao et al., Electroreduction reaction mechanism of carbon dioxide to C_2 products via Cu/Au bimetallic catalysis: a theoretical prediction. J. Phys. Chem. Lett. **11**(16), 6593–6599 (2020). https://doi.org/10.1021/acs.jpclett.0c01970
130. T. Zhang, Y. Qiu, P. Yao, X. Li, H. Zhang, Bi-modified Zn catalyst for efficient CO_2 electrochemical reduction to formate. ACS Sustain. Chem. Eng. **7**(18), 15190–15196 (2019). https://doi.org/10.1021/acssuschemeng.9b01985
131. W. Luc, C. Collins, S. Wang, H. Xin, K. He et al., Ag–Sn bimetallic catalyst with a core–shell structure for CO_2 reduction. J. Am. Chem. Soc. **139**(5), 1885–1893 (2017). https://doi.org/10.1021/jacs.6b10435
132. W. Zhang, Q. Qin, L. Dai, R. Qin, X. Zhao et al., Electrochemical reduction of carbon dioxide to methanol on hierarchical Pd/SnO_2 nanosheets with abundant Pd–O–Sn interfaces. Angew. Chem. Int. Ed. **57**(30), 9475–9479 (2018). https://doi.org/10.1002/anie.201804142
133. W. Tan, B. Cao, W. Xiao, M. Zhang, S. Wang et al., Electrochemical reduction of CO_2 on hollow cubic Cu_2O@Au nanocomposites. Nanoscale Res. Lett. **14**, 63 (2019). https://doi.org/10.1186/s11671-019-2892-3
134. D. Gao, Y. Zhang, Z. Zhou, F. Cai, X. Zhao et al., Enhancing CO_2 electroreduction with the metal–oxide interface. J. Am. Chem. Soc. **139**(16), 5652–5655 (2017). https://doi.org/10.1021/jacs.7b00102
135. X. Huang, J. Song, H. Wu, C. Xie, M. Hua et al., Ordered-mesoporous-carbon-confined Pb/PbO composites: superior electrocatalysts for CO_2 reduction. ChemSusChem **13**(23), 6346–6352 (2020). https://doi.org/10.1002/cssc.202000329
136. F. Lyu, M. Cao, A. Mahsud, Q. Zhang, Interfacial engineering of noble metals for electrocatalytic methanol and ethanol oxidation. J. Mater. Chem. A **8**, 15445–15457 (2020). https://doi.org/10.1039/D0TA03199B
137. K. Ye, Z. Zhou, J. Shao, L. Lin, D. Gao et al., In situ reconstruction of a hierarchical Sn–Cu/SnO_x core/shell catalyst for high-performance CO_2 electroreduction. Angew. Chem. Int. Ed. **59**(12), 4814–4821 (2020). https://doi.org/10.1002/anie.201916538
138. Z. Han, C. Choi, H. Tao, Q. Fan, Y. Gao et al., Tuning the Pd-catalyzed electroreduction of CO_2 to CO with reduced overpotential. Catal. Sci. Technol. **8**(15), 3894–3900 (2018). https://doi.org/10.1039/C8CY01037D
139. S. Gao, Y. Lin, X. Jiao, Y. Sun, Q. Luo et al., Partially oxidized atomic cobalt layers for carbon dioxide electroreduction to liquid fuel. Nature **529**, 68–71 (2016). https://doi.org/10.1038/nature16455
140. X. Zong, J. Zhang, J. Zhang, W. Luo, A. Züttel et al., Synergistic Cu/CeO_2 carbon nanofiber catalysts for efficient CO_2 electroreduction. Electrochem. Commun. **114**, 106716 (2020). https://doi.org/10.1016/j.elecom.2020.106716
141. S.B. Varandili, J. Huang, E. Oveisi, G.L. De Gregorio, M. Mensi et al., Synthesis of Cu/CeO_{2-x} nanocrystalline heterodimers with interfacial active sites to promote CO_2 electroreduction. ACS Catal. **9**(6), 5035–5046 (2019). https://doi.org/10.1021/acscatal.9b00010
142. J. Albo, A. Sáez, J. Solla-Gullón, V. Montiel, A. Irabien, Production of methanol from CO_2 electroreduction at Cu_2O and Cu_2O/ZnO-based electrodes in aqueous solution. Appl. Catal. B-Environ. **176–177**, 709–717 (2015). https://doi.org/10.1016/j.apcatb.2015.04.055
143. Q. Zhao, C. Zhang, R. Hu, Z. Du, J. Gu et al., Selective etching quaternary max phase toward single atom copper immobilized mxene ($Ti_3C_2Cl_x$) for efficient CO_2 electroreduction to methanol. ACS Nano **15**(3), 4927–4936 (2021). https://doi.org/10.1021/acsnano.0c09755
144. M. Casavola, R. Buonsanti, G. Caputo, P.D. Cozzoli, Colloidal strategies for preparing oxide-based hybrid nanocrystals. Eur. J. Inorg. Chem. **2008**(4), 837–854 (2008). https://doi.org/10.1002/ejic.200701047
145. A. Bhowmik, H.A. Hansen, T. Vegge, Electrochemical reduction of CO_2 on $Ir_xRu_{(1-x)}O_2$(110) surfaces. ACS Catal. **7**(12), 8502–8513 (2017). https://doi.org/10.1021/acscatal.7b02914
146. A. Bhowmik, T. Vegge, H.A. Hansen, Descriptors and thermodynamic limitations of electrocatalytic carbon dioxide reduction on rutile oxide surfaces. ChemSusChem **9**(22), 3230–3243 (2016). https://doi.org/10.1002/cssc.201600845
147. X. Hong, K. Chan, C. Tsai, J.K. Nørskov, How doped MoS_2 breaks transition-metal scaling relations for CO_2 electrochemical reduction. ACS Catal. **6**(7), 4428–4437 (2016). https://doi.org/10.1021/acscatal.6b00619
148. A. Bhowmik, H.A. Hansen, T. Vegge, Role of CO* as a spectator in CO_2 electroreduction on RuO_2. J. Phys. Chem. C **121**(34), 18333–18343 (2017). https://doi.org/10.1021/acs.jpcc.7b04242
149. Z.W. Ulissi, A.J. Medford, T. Bligaard, J.K. Norskov, To address surface reaction network complexity using scaling

 https://doi.org/10.1007/s40820-021-00738-9

relations machine learning and DFT calculations. Nat. Commun. **8**, 14621 (2017). https://doi.org/10.1038/ncomms14621

150. Y. Li, Q. Sun, Recent advances in breaking scaling relations for effective electrochemical conversion of CO_2. Adv. Energy Mater. **6**(17), 1600463 (2016). https://doi.org/10.1002/aenm.201600463
151. C.W. Lee, S.J. Shin, H. Jung, D.L.T. Nguyen, S.Y. Lee et al., Metal–oxide interfaces for selective electrochemical C–C coupling reactions. ACS Energy Lett. **4**(9), 2241–2248 (2019). https://doi.org/10.1021/acsenergylett.9b01721
152. J. Fu, D. Ren, M. Xiao, K. Wang, Y. Deng et al., Manipulating Au–CeO_2 interfacial structure toward ultrahigh mass activity and selectivity for CO_2 reduction. ChemSusChem **13**(24), 6621–6628 (2020). https://doi.org/10.1002/cssc.202002133
153. S.D. Senanayake, D. Stacchiola, J. Evans, M. Estrella, L. Barrio et al., Probing the reaction intermediates for the water–gas shift over inverse CeO_x/Au(111) catalysts. J. Catal. **271**(2), 392–400 (2010). https://doi.org/10.1016/j.jcat.2010.02.024
154. M.A. Henderson, C.L. Perkins, M.H. Engelhard, S. Thevuthasan, C.H.F. Peden, Redox properties of water on the oxidized and reduced surfaces of CeO_2(111). Surf. Sci. **526**(1–2), 1–18 (2003). https://doi.org/10.1016/S0039-6028(02)02657-2
155. Z. Cai, Y. Wu, Z. Wu, L. Yin, Z. Weng et al., Unlocking bifunctional electrocatalytic activity for CO_2 reduction reaction by win–win metal–oxide cooperation. ACS Energy Lett. **3**(11), 2816–2822 (2018). https://doi.org/10.1021/acsenergylett.8b01767
156. D. Gao, H. Zhou, F. Cai, D. Wang, Y. Hu et al., Switchable CO_2 electroreduction via engineering active phases of Pd nanoparticles. Nano Res. **10**, 2181–2191 (2017). https://doi.org/10.1007/s12274-017-1514-6
157. X. Min, M.W. Kanan, Pd-catalyzed electrohydrogenation of carbon dioxide to formate: high mass activity at low overpotential and identification of the deactivation pathway. J. Am. Chem. Soc. **137**(14), 4701–4708 (2015). https://doi.org/10.1021/ja511890h
158. Y. Wu, X. Yuan, Z. Tao, H. Wang, Bifunctional electrocatalysis for CO_2 reduction via surface capping-dependent metal–oxide interactions. Chem. Commun. **55**(60), 8864–8867 (2019). https://doi.org/10.1039/C9CC02934F
159. Z. Tao, Z. Wu, X. Yuan, Y. Wu, H. Wang, Copper–gold interactions enhancing formate production from electrochemical CO_2 reduction. ACS Catal. **9**(12), 10894–10898 (2019). https://doi.org/10.1021/acscatal.9b03158
160. X. Yuan, Y. Wu, B. Jiang, Z. Wu, Z. Tao et al., Interface engineering of silver-based heterostructures for CO_2 reduction reaction. ACS Appl. Mater. Interfaces **12**(50), 56642–56649 (2020). https://doi.org/10.1021/acsami.0c19031
161. N. Liu, Y. Zhao, S. Zhou, J. Zhao, CO_2 reduction on p-block metal oxide overlayers on metal substrates-2D MgO as a prototype. J. Mater. Chem. A **8**(11), 5688–5698 (2020). https://doi.org/10.1039/C9TA13864A
162. L. Zhai, C. Cui, Y. Zhao, X. Zhu, J. Han et al., Titania-modified silver electrocatalyst for selective CO_2 reduction to CH_3OH and CH_4 from DFT study. J. Phys. Chem. C **121**(30), 16275–16282 (2017). https://doi.org/10.1021/acs.jpcc.7b03314
163. W. Zheng, S. Nayak, W. Yuan, Z. Zeng, X. Hong et al., A tunable metal–polyaniline interface for efficient carbon dioxide electro-reduction to formic acid and methanol in aqueous solution. Chem. Commun. **52**(96), 13901–13904 (2016). https://doi.org/10.1039/C6CC07212G
164. H. Wang, Y.K. Tzeng, Y. Ji, Y. Li, J. Li et al., Synergistic enhancement of electrocatalytic CO_2 reduction to C_2 oxygenates at nitrogen-doped nanodiamonds/Cu interface. Nat. Nanotechnol. **15**, 131–137 (2020). https://doi.org/10.1038/s41565-019-0603-y
165. G. Hu, Z. Wu, S. Dai, D. Jiang, Interface engineering of earth-abundant transition metals using boron nitride for selective electroreduction of CO_2. ACS Appl. Mater. Interfaces. **10**(7), 6694–6700 (2018). https://doi.org/10.1021/acsami.7b17600
166. H. Shang, T. Wang, J. Pei, Z. Jiang, D. Zhou et al., Design of a single-atom Indium$^{\delta+}$–N_4 interface for efficient electroreduction of CO_2 to formate. Angew. Chem. Int. Ed. **59**(50), 22465–22469 (2020). https://doi.org/10.1002/anie.202010903
167. C. Genovese, M.E. Schuster, E.K. Gibson, D. Gianolio, V. Posligua et al., Operando spectroscopy study of the carbon dioxide electro-reduction by iron species on nitrogen-doped carbon. Nat. Commun. **9**, 935 (2018). https://doi.org/10.1038/s41467-018-03138-7
168. S. Lee, D. Kim, J. Lee, Electrocatalytic production of C_3–C_4 compounds by conversion of CO_2 on a chloride-induced Bi-phasic Cu_2O–Cu catalyst. Angew. Chem. Int. Ed. **54**(49), 14701–14705 (2015). https://doi.org/10.1002/anie.201505730
169. C. Chen, J. Wan, B. Yeo, Electrochemical reduction of carbon dioxide to ethane using nanostructured Cu_2O-derived copper catalyst and palladium(II) chloride. J. Phys. Chem. C **119**(48), 26875–268582 (2015). https://doi.org/10.1021/acs.jpcc.5b09144
170. H. Mistry, A.S. Varela, C.S. Bonifacio, I. Zegkinoglou, I. Sinev et al., Highly selective plasma-activated copper catalysts for carbon dioxide reduction to ethylene. Nat. Commun. **7**, 12123 (2016). https://doi.org/10.1038/ncomms12123
171. A.D. Handoko, C.W. Ong, Y. Huang, Z.G. Lee, L. Lin et al., Mechanistic insights into the selective electroreduction of carbon dioxide to ethylene on Cu_2O-derived copper catalysts. J. Phys. Chem. C **120**(36), 20058–20067 (2016). https://doi.org/10.1021/acs.jpcc.6b07128
172. A. Dutta, M. Rahaman, N.C. Luedi, M. Mohos, P. Broekmann, Morphology matters: tuning the product distribution of CO_2 electroreduction on oxide-derived Cu foam catalysts. ACS Catal. **6**(6), 3804–3814 (2016). https://doi.org/10.1021/acscatal.6b00770
173. D. Gao, I. Zegkinoglou, N.J. Divins, F. Scholten, I. Sinev et al., Plasma-activated copper nanocube catalysts for efficient carbon dioxide electroreduction to hydrocarbons and

alcohols. ACS Nano **11**(5), 4825–4831 (2017). https://doi.org/10.1021/acsnano.7b01257

174. D. Ren, Y. Deng, A.D. Handoko, C. Chen, S. Malkhandi et al., Selective electrochemical reduction of carbon dioxide to ethylene and ethanol on copper(I) oxide catalysts. ACS Catal. **5**(5), 2814–2821 (2015). https://doi.org/10.1021/cs502128q
175. A. Loiudice, P. Lobaccaro, E.A. Kamali, T. Thao, B.H. Huang et al., Tailoring copper nanocrystals towards C_2 products in electrochemical CO_2 reduction. Angew. Chem. Int. Ed. **55**(19), 5789–5792 (2016). https://doi.org/10.1002/anie.201601582
176. Y. Hori, I. Takahashi, O. Koga, N. Hoshi, Electrochemical reduction of carbon dioxide at various series of copper single crystal electrodes. J. Mol. Catal. A-Chem. **199**(1–2), 39–47 (2003)
177. D. Kim, C.S. Kley, Y. Li, P. Yang, Copper nanoparticle ensembles for selective electroreduction of CO_2 to C_2–C_3 products. Proc. Natl. Acad. Sci. USA **114**(40), 10560–10565 (2017). https://doi.org/10.1073/pnas.1711493114
178. C.W. Li, J. Ciston, M.W. Kanan, Electroreduction of carbon monoxide to liquid fuel on oxide-derived nanocrystalline copper. Nature **508**, 504–507 (2014). https://doi.org/10.1038/nature13249
179. C.S. Diercks, S. Lin, N. Kornienko, E.A. Kapustin, E.M. Nichols et al., Reticular electronic tuning of porphyrin active sites in covalent organic frameworks for electrocatalytic carbon dioxide reduction. J. Am. Chem. Soc. **140**(3), 1116–1122 (2018). https://doi.org/10.1021/jacs.7b11940
180. A.J. Garza, A.T. Bell, M. Head-Gordon, Is subsurface oxygen necessary for the electrochemical reduction of CO_2 on copper? J. Phys. Chem. Lett. **9**(3), 601–606 (2018). https://doi.org/10.1021/acs.jpclett.7b03180
181. F. Cavalca, R. Ferragut, S. Aghion, A. Eilert, O. Diaz-Morales et al., Nature and distribution of stable subsurface oxygen in copper electrodes during electrochemical CO_2 reduction. J. Phys. Chem. C **121**(45), 25003–25009 (2017). https://doi.org/10.1021/acs.jpcc.7b08278
182. L. Ma, W. Hu, Q. Pan, L. Zou, Z. Zou et al., Polyvinyl alcohol-modified gold nanoparticles with record-high activity for electrochemical reduction of CO_2 to CO. J. CO2 Util. **34**, 108–114 (2019). https://doi.org/10.1016/j.jcou.2019.06.002
183. H. Yang, S. Hung, S. Liu, K. Yuan, S. Miao et al., Atomically dispersed Ni(I) as the active site for electrochemical CO_2 reduction. Nat. Energy **3**, 140–147 (2018). https://doi.org/10.1038/s41560-017-0078-8
184. J. Yang, W. Li, D. Wang, Y. Li, Electronic metal–support interaction of single-atom catalysts and applications in electrocatalysis. Adv. Mater. **32**(49), 2003300 (2020). https://doi.org/10.1002/adma.202003300
185. H. Shang, W. Sun, R. Sui, J. Pei, L. Zheng et al., Engineering isolated Mn–N_2C_2 atomic interface sites for efficient bifunctional oxygen reduction and evolution reaction. Nano Lett. **20**(7), 5443–5450 (2020). https://doi.org/10.1021/acs.nanolett.0c01925
186. F. Yang, P. Song, X. Liu, B. Mei, W. Xing et al., Highly efficient CO_2 electroreduction on ZnN_4-based single-atom catalyst. Angew. Chem. Int. Ed. **57**(38), 12303–12307 (2018). https://doi.org/10.1002/anie.201805871
187. S. Ji, Y. Qu, T. Wang, Y. Chen, G. Wang et al., Rare-earth single erbium atoms for enhanced photocatalytic CO_2 reduction. Angew. Chem. Int. Ed. **59**(26), 10651–10657 (2020). https://doi.org/10.1002/anie.202003623
188. W. Ju, A. Bagger, G. Hao, A.S. Varela, I. Sinev et al., Understanding activity and selectivity of metal–nitrogen-doped carbon catalysts for electrochemical reduction of CO_2. Nat. Commun. **8**, 944 (2017). https://doi.org/10.1038/s41467-017-01035-z
189. X. Cui, F. Shi, Selective conversion of CO_2 by single-site catalysts. Acta Phys-Chim. Sin. **37**(5), 2006080 (2020). https://doi.org/10.3866/PKU.WHXB202006080
190. D. Wu, X. Wang, L. Shi, K. Jiang, M. Wang et al., Iron clusters boosted performance in electrocatalytic carbon dioxide conversion. J. Mater. Chem. A **8**(41), 21661–21667 (2020). https://doi.org/10.1039/D0TA07867K
191. G. Chen, C. Xu, X. Huang, J. Ye, L. Gu et al., Interfacial electronic effects control the reaction selectivity of platinum catalysts. Nat. Mater. **15**, 564–569 (2016). https://doi.org/10.1038/nmat4555
192. L. Zhang, F. Mao, L. Zheng, H. Wang, X. Yang et al., Tuning metal catalyst with metal–C_3N_4 interaction for efficient CO_2 electroreduction. ACS Catal. **8**(12), 11035–11041 (2018). https://doi.org/10.1021/acscatal.8b03789
193. J. Tian, R. Wang, M. Shen, X. Ma, H. Yao et al., Bi–Sn oxides for highly selective CO_2 electroreduction to formate in a wide potential window. ChemSusChem (2021). https://doi.org/10.1002/cssc.202100543
194. J. Wu, Y. Xie, S. Du, Z. Ren, P. Yu et al., Heterophase engineering of SnO_2/Sn_3O_4 drives enhanced carbon dioxide electrocatalytic reduction to formic acid. Sci. China Mater. **63**, 2314–2324 (2020). https://doi.org/10.1007/s40843-020-1361-3
195. Y.W. Choi, F. Scholten, I. Sinev, B. Roldan Cuenya, Enhanced stability and CO/formate selectivity of plasma-treated SnO_x/AgO_x catalysts during CO_2 electroreduction. J. Am. Chem. Soc. **141**(13), 5261–5266 (2019). https://doi.org/10.1021/jacs.8b12766
196. A. Dutta, A. Kuzume, M. Rahaman, S. Vesztergom, P. Broekmann, Monitoring the chemical state of catalysts for CO_2 electroreduction: an in operando study. ACS Catal. **5**(12), 7498–7502 (2015). https://doi.org/10.1021/acscatal.5b02322
197. S. Chu, X. Yan, C. Choi, S. Hong, A.W. Robertson et al., Stabilization of Cu^+ by tuning a CuO–CeO_2 interface for selective electrochemical CO_2 reduction to ethylene. Green Chem. **22**(19), 6540–6546 (2020). https://doi.org/10.1039/D0GC02279A
198. H. Xiao, W.A. Goddard, T. Cheng, Y. Liu, Cu metal embedded in oxidized matrix catalyst to promote CO_2 activation and CO dimerization for electrochemical reduction of CO_2. Proc.

 https://doi.org/10.1007/s40820-021-00738-9

Natl. Acad. Sci. USA **114**(26), 6685–6688 (2017). https://doi.org/10.1073/pnas.1702405114

199. M. Favaro, H. Xiao, T. Cheng, W.A. Goddard, J. Yano et al., Subsurface oxide plays a critical role in CO_2 activation by Cu(111) surfaces to form chemisorbed CO_2, the first step in reduction of CO_2. Proc. Natl. Acad. Sci. USA **114**(26), 6706–6711 (2017). https://doi.org/10.1073/pnas.1701405114
200. X. Yan, C. Chen, Y. Wu, S. Liu, Y. Chen et al., Efficient electroreduction of CO_2 to C_{2+} products on CeO_2 modified CuO. Chem. Sci. **12**(19), 6638–6645 (2021). https://doi.org/10.1039/D1SC01117K
201. Y.J. Sa, C.W. Lee, S.Y. Lee, J. Na, U. Lee et al., Catalyst–electrolyte interface chemistry for electrochemical CO_2 reduction. Chem. Soc. Rev. **49**(18), 6632–6665 (2020). https://doi.org/10.1039/D0CS00030B
202. F. Li, A. Thevenon, A. Rosas-Hernandez, Z. Wang, Y. Li et al., Molecular tuning of CO_2-to-ethylene conversion. Nature **577**, 509–513 (2020). https://doi.org/10.1038/s41586-019-1782-2
203. F. Li, Y.C. Li, Z. Wang, J. Li, D.H. Nam et al., Cooperative CO_2-to-ethanol conversion via enriched intermediates at molecule–metal catalyst interfaces. Nat. Catal. **3**, 75–82 (2019). https://doi.org/10.1038/s41929-019-0383-7
204. J.R. Pankhurst, P. Iyengar, A. Loiudice, M. Mensi, R. Buonsanti, Metal–ligand bond strength determines the fate of organic ligands on the catalyst surface during the electrochemical CO_2 reduction reaction. Chem. Sci. **11**(34), 9296–9302 (2020). https://doi.org/10.1039/D0SC03061A
205. Z. Cao, D. Kim, D. Hong, Y. Yu, J. Xu et al., A molecular surface functionalization approach to tuning nanoparticle electrocatalysts for carbon dioxide reduction. J. Am. Chem. Soc. **138**(26), 8120–8125 (2016). https://doi.org/10.1021/jacs.6b02878
206. S. Li, A.V. Nagarajan, Y. Li, D.R. Kauffman, G. Mpourmpakis et al., The role of ligands in atomically precise nanocluster-catalyzed CO_2 electrochemical reduction. Nanoscale **13**(4), 2333–2337 (2021). https://doi.org/10.1039/D0NR07832H
207. Y. Fang, J.C. Flake, Electrochemical reduction of CO_2 at functionalized Au electrodes. J. Am. Chem. Soc. **139**(9), 3399–3405 (2017). https://doi.org/10.1021/jacs.6b11023
208. X. Cai, H. Liu, X. Wei, Z. Yin, J. Chu et al., Molecularly defined interface created by porous polymeric networks on gold surface for concerted and selective CO_2 reduction. ACS Sustain. Chem. Eng. **6**(12), 17277–17283 (2018). https://doi.org/10.1021/acssuschemeng.8b04691
209. Y. Zhou, L. Zheng, D. Yang, H. Yang, Q. Lu et al., Enhancing CO_2 electrocatalysis on 2D porphyrin-based metal–organic framework nanosheets coupled with visible-light. Small Methods **5**(2), 2000991 (2021). https://doi.org/10.1002/smtd.202000991
210. A. Wagner, K.H. Ly, N. Heidary, I. Szabo, T. Foldes et al., Host-guest chemistry meets electrocatalysis: Cucurbit[6]uril on a Au surface as a hybrid system in CO_2 reduction. ACS Catal. **10**(1), 751–761 (2020). https://doi.org/10.1021/acscatal.9b04221
211. Y.T. Guntern, J.R. Pankhurst, J. Vavra, M. Mensi, V. Mantella et al., Nanocrystal/metal–organic framework hybrids as electrocatalytic platforms for CO_2 conversion. Angew. Chem. Int. Ed. **58**(36), 12632–12639 (2019). https://doi.org/10.1002/anie.201905172
212. D.H. Nam, P.D. Luna, A. Rosas-Hernandez, A. Thevenon, F. Li et al., Molecular enhancement of heterogeneous CO_2 reduction. Nat. Mater. **19**, 266–276 (2020). https://doi.org/10.1038/s41563-020-0610-2
213. M. Ma, B.J. Trzesniewski, J. Xie, W.A. Smith, Selective and efficient reduction of carbon dioxide to carbon monoxide on oxide-derived nanostructured silver electrocatalysts. Angew. Chem. Int. Ed. **55**(33), 9748–9752 (2016). https://doi.org/10.1002/anie.201604654
214. M.R. Singh, E.L. Clark, A.T. Bell, Effects of electrolyte, catalyst, and membrane composition and operating conditions on the performance of solar-driven electrochemical reduction of carbon dioxide. Phys. Chem. Chem. Phys. **17**(29), 18924–18936 (2015). https://doi.org/10.1039/C5CP03283K
215. R.M. Aran-Ais, D. Gao, B. Roldan Cuenya, Structure- and electrolyte-sensitivity in CO_2 electroreduction. Acc. Chem. Res. **51**(11), 2906–2917 (2018). https://doi.org/10.1021/acs.accounts.8b00360
216. D. Gao, R.M. Arán-Ais, H.S. Jeon, B. Roldan Cuenya, Rational catalyst and electrolyte design for CO_2 electroreduction towards multicarbon products. Nat. Catal. **2**, 198–210 (2019). https://doi.org/10.1038/s41929-019-0235-5
217. Y. Hori, A. Murata, R. Takahashi, Formation of hydrocarbons in the electrochemical reduction of carbon dioxide at a copper electrode in aqueous solution. J. Chem. Soc. Faraday Trans. 1 **85**(8), 2309–2326 (1989). https://doi.org/10.1039/F19898502309
218. S. Zhu, B. Jiang, W. Cai, M. Shao, Direct observation on reaction intermediates and the role of bicarbonate anions in CO_2 electrochemical reduction reaction on Cu surfaces. J. Am. Chem. Soc. **139**(44), 15664–15667 (2017). https://doi.org/10.1021/jacs.7b10462
219. A. Wuttig, Y. Yoon, J. Ryu, Y. Surendranath, Bicarbonate is not a general acid in Au-catalyzed CO_2 electroreduction. J. Am. Chem. Soc. **139**(47), 17109–17113 (2017). https://doi.org/10.1021/jacs.7b08345
220. A. Murata, Y. Hori, Product selectivity affected by cationic species in electrochemical reduction of CO_2 and CO at a Cu electrode. Bull. Chem. Soc. Jpn. **64**, 123–127 (1991). https://doi.org/10.1246/bcsj.64.123
221. M.R. Thorson, K.I. Siil, P.J.A. Kenis, Effect of cations on the electrochemical conversion of CO_2 to CO. J. Electrochem. Soc. **160**, F69 (2012). https://doi.org/10.1149/2.052301jes
222. D. Gao, I.T. McCrum, S. Deo, Y.W. Choi, F. Scholten et al., Activity and selectivity control in CO_2 electroreduction to multicarbon products over CuO_x catalysts via electrolyte design. ACS Catal. **8**(11), 10012–10020 (2018). https://doi.org/10.1021/acscatal.8b02587
223. A. Schizodimou, G. Kyriacou, Acceleration of the reduction of carbon dioxide in the presence of multivalent cations.

Electrochim. Acta **78**, 171–176 (2012). https://doi.org/10.1016/j.electacta.2012.05.118

224. M. Dunwell, Q. Lu, J.M. Heyes, J. Rosen, J.G. Chen et al., The central role of bicarbonate in the electrochemical reduction of carbon dioxide on gold. J. Am. Chem. Soc. **139**(10), 3774–3783 (2017). https://doi.org/10.1021/jacs.6b13287
225. M.R. Singh, Y. Kwon, Y. Lum, J.W. Ager, A.T. Bell, Hydrolysis of electrolyte cations enhances the electrochemical reduction of CO_2 over Ag and Cu. J. Am. Chem. Soc. **138**(39), 13006–13012 (2016). https://doi.org/10.1021/jacs.6b07612
226. O. Ayemoba, A. Cuesta, Spectroscopic evidence of size-dependent buffering of interfacial pH by cation hydrolysis during CO_2 electroreduction. ACS Appl. Mater. Interfaces **9**(33), 27377–27382 (2017). https://doi.org/10.1021/acsami.7b07351
227. S. Ringe, E.L. Clark, J. Resasco, A. Walton, B. Seger et al., Understanding cation effects in electrochemical CO_2 reduction. Energy Environ. Sci. **12**(10), 3001–3014 (2019). https://doi.org/10.1039/C9EE01341E
228. Y. Hori, H. Konishi, T. Futamura, A. Murata, O. Koga et al., "Deactivation of copper electrode" in electrochemical reduction of CO_2. Electrochim. Acta **50**(27), 5354–5369 (2005). https://doi.org/10.1016/j.electacta.2005.03.015
229. A. Wuttig, Y. Surendranath, Impurity ion complexation enhances carbon dioxide reduction catalysis. ACS Catal. **5**(7), 4479–4484 (2015). https://doi.org/10.1021/acscatal.5b00808
230. D.H. Won, H. Shin, M.W. Chung, H. Jung, K.H. Chae et al., Achieving tolerant CO_2 electro-reduction catalyst in real water matrix. Appl. Catal. B-Environ. **258**, 117961 (2019). https://doi.org/10.1016/j.apcatb.2019.117961
231. J. Resasco, Y. Lum, E. Clark, J.Z. Zeledon, A.T. Bell, Effects of anion identity and concentration on electrochemical reduction of CO_2. ChemElectroChem **5**(7), 1064–1072 (2018). https://doi.org/10.1002/celc.201701316
232. A.S. Varela, W. Ju, T. Reier, P. Strasser, Tuning the catalytic activity and selectivity of Cu for CO_2 electroreduction in the presence of halides. ACS Catal. **6**(4), 2136–2144 (2016). https://doi.org/10.1021/acscatal.5b02550
233. D. Gao, F. Scholten, B. Roldan Cuenya, Improved CO_2 electroreduction performance on plasma-activated Cu catalysts via electrolyte design: Halide effect. ACS Catal. **7**(8), 5112–5120 (2017). https://doi.org/10.1021/acscatal.7b01416
234. Y. Huang, C.W. Ong, B.S. Yeo, Effects of electrolyte anions on the reduction of carbon dioxide to ethylene and ethanol on copper (100) and (111) surfaces. ChemSusChem **11**(18), 3299–3306 (2018). https://doi.org/10.1002/cssc.201801078
235. D. Gao, I. Sinev, F. Scholten, R.M. Aran-Ais, N.J. Divins et al., Selective CO_2 electroreduction to ethylene and multicarbon alcohols via electrolyte-driven nanostructuring. Angew. Chem. Int. Ed. **58**(47), 17047–17053 (2019). https://doi.org/10.1002/anie.201910155
236. F.S. Roberts, K.P. Kuhl, A. Nilsson, High selectivity for ethylene from carbon dioxide reduction over copper nanocube electrocatalysts. Angew. Chem. Int. Ed. **54**(17), 5179–5182 (2015). https://doi.org/10.1002/anie.201412214
237. Y.C. Hsieh, S.D. Senanayake, Y. Zhang, W. Xu, D.E. Polyansky, Effect of chloride anions on the synthesis and enhanced catalytic activity of silver nanocoral electrodes for CO_2 electroreduction. ACS Catal. **5**(9), 5349–5356 (2015). https://doi.org/10.1021/acscatal.5b01235
238. D.L.T. Nguyen, M.S. Jee, D.H. Won, H.S. Oh, B.K. Min et al., Effect of halides on nanoporous Zn-based catalysts for highly efficient electroreduction of CO_2 to CO. Catal. Commun. **114**, 109–113 (2018). https://doi.org/10.1016/j.catcom.2018.06.020
239. Y.C. Hsieh, L.E. Betancourt, S.D. Senanayake, E. Hu, Y. Zhang et al., Modification of CO_2 reduction activity of nanostructured silver electrocatalysts by surface halide anions. ACS Appl. Energy Mater. **2**(1), 102–109 (2019). https://doi.org/10.1021/acsaem.8b01692
240. Y. Zhang, L. Liu, L. Shi, T. Yang, D. Niu et al., Enhancing CO_2 electroreduction on nanoporous silver electrode in the presence of halides. Electrochim. Acta **313**, 561–569 (2019). https://doi.org/10.1016/j.electacta.2019.04.175
241. H. Fu, L. Zhang, L. Zheng, P. Liu, H. Zhao et al., Enhanced CO_2 electroreduction performance over Cl-modified metal catalysts. J. Mater. Chem. A **7**(20), 12420–12435 (2019). https://doi.org/10.1039/C9TA02223F
242. M. Zhao, H. Tang, Q. Yang, Y. Gu, H. Zhu et al., Inhibiting hydrogen evolution using a chloride adlayer for efficient electrochemical CO_2 reduction on Zn electrodes. ACS Appl. Mater. Interfaces **12**(4), 4565–4571 (2020). https://doi.org/10.1021/acsami.9b22811
243. M. Cho, J.T. Song, S. Back, Y. Jung, J. Oh, The role of adsorbed CN and Cl on an Au electrode for electrochemical CO_2 reduction. ACS Catal. **8**(2), 1178–1185 (2018). https://doi.org/10.1021/acscatal.7b03449
244. N. Ikemiya, K. Natsui, K. Nakata, Y. Einaga, Effect of alkali-metal cations on the electrochemical reduction of carbon dioxide to formic acid using boron-doped diamond electrodes. RSC Adv. **7**(36), 22510–22514 (2017). https://doi.org/10.1039/C7RA03370B
245. M. Tomisaki, S. Kasahara, K. Natsui, N. Ikemiya, Y. Einaga, Switchable product selectivity in the electrochemical reduction of carbon dioxide using boron-doped diamond electrodes. J. Am. Chem. Soc. **141**(18), 7414–7420 (2019). https://doi.org/10.1021/jacs.9b01773
246. M. Tomisaki, K. Natsui, N. Ikemiya, K. Nakata, Y. Einaga, Influence of electrolyte on the electrochemical reduction of carbon dioxide using boron-doped diamond electrodes. ChemistrySelect **3**(36), 10209–10213 (2018). https://doi.org/10.1002/slct.201801546
247. P. Lobaccaro, M.R. Singh, E.L. Clark, Y. Kwon, A.T. Bell et al., Effects of temperature and gas–liquid mass transfer on the operation of small electrochemical cells for the quantitative evaluation of CO_2 reduction electrocatalysts. Phys. Chem. Chem. Phys. **18**(38), 26777–26785 (2016). https://doi.org/10.1039/C6CP05287H
248. J. Li, G. Chen, Y. Zhu, Z. Liang, A. Pei et al., Efficient electrocatalytic CO_2 reduction on a three-phase interface.

 https://doi.org/10.1007/s40820-021-00738-9

Nat. Catal. **1**, 592–600 (2018). https://doi.org/10.1038/s41929-018-0108-3

249. D. Wakerley, S. Lamaison, F. Ozanam, N. Menguy, D. Mercie et al., Bio-inspired hydrophobicity promotes CO_2 reduction on a Cu surface. Nat. Mater. **18**, 1222–1227 (2019). https://doi.org/10.1038/s41563-019-0445-x
250. F. Lei, W. Liu, Y. Sun, J. Xu, K. Liu et al., Metallic tin quantum sheets confined in graphene toward high-efficiency carbon dioxide electroreduction. Nat. Commun. **7**, 12697 (2016). https://doi.org/10.1038/ncomms12697
251. N. Gupta, M. Gattrell, B. MacDougall, Calculation for the cathode surface concentrations in the electrochemical reduction of CO_2 in $KHCO_3$ solutions. J. Appl. Electrochem. **36**, 161–172 (2006). https://doi.org/10.1007/s10800-005-9058-y
252. J. Ryu, A. Wuttig, Y. Surendranath, Quantification of interfacial pH variation at molecular length scales using a concurrent non-faradaic reaction. Angew. Chem. Int. Ed. **57**(30), 9300–9304 (2018). https://doi.org/10.1002/anie.201802756
253. D. Raciti, M. Mao, C. Wang, Mass transport modelling for the electroreduction of CO_2 on Cu nanowires. Nanotechnology **29**, 044001 (2018). https://doi.org/10.1088/1361-6528/aa9bd7
254. K. Yang, R. Kas, W.A. Smith, In situ infrared spectroscopy reveals persistent alkalinity near electrode surfaces during CO_2 electroreduction. J. Am. Chem. Soc. **141**(40), 15891–15900 (2019). https://doi.org/10.1021/jacs.9b07000
255. A.S. Hall, Y. Yoon, A. Wuttig, Y. Surendranath, Mesostructure-induced selectivity in CO_2 reduction catalysis. J. Am. Chem. Soc. **137**(47), 14834–14837 (2015). https://doi.org/10.1021/jacs.5b08259
256. M.R. Singh, J.D. Goodpaster, A.Z. Weber, M. Head-Gordon, A.T. Bell, Mechanistic insights into electrochemical reduction of CO_2 over Ag using density functional theory and transport models. Proc. Natl. Acad. Sci. USA **114**(42), E8812–E8821 (2017). https://doi.org/10.1073/pnas.1713164114
257. W. Luo, J. Zhang, M. Li, A. Züttel, Boosting CO production in electrocatalytic CO_2 reduction on highly porous Zn catalysts. ACS Catal. **9**(5), 3783–3791 (2019). https://doi.org/10.1021/acscatal.8b05109
258. D. Yang, G. Wang, X. Wang, Photo- and thermo-coupled electrocatalysis in carbon dioxide and methane conversion. Sci. China Mater. **62**, 1369–1373 (2019). https://doi.org/10.1007/s40843-019-9455-3
259. J. Resasco, L.D. Chen, E. Clark, C. Tsai, C. Hahn et al., Promoter effects of alkali metal cations on the electrochemical reduction of carbon dioxide. J. Am. Chem. Soc. **139**(32), 11277–11287 (2017). https://doi.org/10.1021/jacs.7b06765
260. C. Yang, Y. Zhu, J. Liu, Y. Qin, H. Wang et al., Defect engineering for electrochemical nitrogen reduction reaction to ammonia. Nano Energy **77**, 105126 (2020). https://doi.org/10.1016/j.nanoen.2020.105126
261. Y. Zhu, X. Cui, H. Liu, Z. Guo, Y. Dang et al., Tandem catalysis in electrochemical CO_2 reduction reaction. Nano Res. (2021). https://doi.org/10.1007/s12274-021-3448-2
262. D. Yang, S. Zuo, H. Yang, X. Wang, Single-unit-cell catalysis of CO_2 electroreduction over sub-1 nm Cu_9S_5 nanowires. Adv. Energy Mater. **11**(16), 2100272 (2021). https://doi.org/10.1002/aenm.202100272
263. D. Yang, H. Yu, T. He, S. Zuo, X. Liu et al., Visible-light-switched electron transfer over single porphyrin–metal atom center for highly selective electroreduction of carbon dioxide. Nat. Commun. **10**, 3844 (2019). https://doi.org/10.1038/s41467-019-11817-2
264. D. Yang, S. Zuo, H. Yang, Y. Zhou, X. Wang, Freestanding millimeter-scale porphyrin-based monoatomic layers with 0.28 nm thickness for CO_2 electrocatalysis. Angew. Chem. Int. Ed. **59**(43), 18954–18957 (2020). https://doi.org/10.1002/anie.202006899
265. M. Xie, B. Xia, Y. Li, Y. Yan, Y. Yang et al., Amino acid modified copper electrodes for the enhanced selective electroreduction of carbon dioxide towards hydrocarbons. Energy Environ. Sci. **9**(5), 1687–1695 (2016). https://doi.org/10.1039/C5EE03694A